Array scattering resonance in the context of Foldy's approximation

DOI:
10.1098/rspa.2022.0604

Document Version
Final published version

PROCEEDINGS A

royalsocietypublishing.org/journal/rspa

Research

Cite this article: Nethercote MA, Kisil AV, Thompson I, Assier RC. 2022 Array scattering resonance in the context of Foldy's approximation. *Proc. R. Soc. A* **478**: 20220604. https://doi.org/10.1098/rspa.2022.0604

Received: 13 September 2022
Accepted: 18 November 2022

Subject Areas:
applied mathematics, mathematical physics, acoustics

Keywords:
multiple scattering, resonance, infinite arrays, semi-infinite arrays

Author for correspondence:
M. A. Nethercote
e-mail:
matthew.nethercote@manchester.ac.uk

Array scattering resonance in the context of Foldy's approximation

M. A. Nethercote[1], A. V. Kisil[1], I. Thompson[2] and R. C. Assier[1]

[1]Department of Mathematics, University of Manchester, Manchester, UK
[2]Department of Mathematics, University of Liverpool, Liverpool, UK

MAN, 0000-0002-7566-1693; AVK, 0000-0001-7652-5880; IT , 0000-0001-5537-450X; RCA, 0000-0001-9848-3482

This article provides an overview of resonance phenomena in wave scattering by infinite and semi-infinite periodic arrays of small cylindrical scatterers, in the context of Foldy's approximation. It briefly summarizes well-known results from the literature. Moreover, for infinite arrays, the asymptotics of the resonant wave amplitudes in the double resonance case is investigated. This leads to the rediscovery of non-uniqueness of the solution in this context, and to a discussion of the validity of Foldy's approximation for double resonance. For semi-infinite arrays, a new and improved uniform far-field approximation is derived, uniqueness issues are considered and the validity of Foldy's approximation is discussed.

1. Introduction

The study of wave propagation in periodic structures has benefited greatly from the design of metamaterials and their subsequent benefits in noise management. This is because metamaterials are usually modelled as a periodic arrangement of small segments called unit cells. Examples of these metamaterial models include designs in three dimensions (see [1–3]) as well as the much thinner and lighter two-dimensional metasurfaces (see [4–7]) and metagratings [8]. There are many articles that study diffraction by periodic structures including infinite arrays [9–12] and semi-infinite arrays [13–15].

THE ROYAL SOCIETY PUBLISHING

One open avenue of investigation in the literature is the different ways to change the structure of the unit cells since doing so can drastically affect the overall scattering. For example, Lynott *et al*. [16] use the boundary element method to calculate the reflection and transmission coefficients associated with infinite arrays of various smooth-shaped scatterers. Alternatively, one can keep simple unit cells but change the array configuration to study the effects of edges. This was the intention of our previous work [17] where we studied a wedge interface consisting of point scatterers. The notation and results of [17] will be used in this work as a starting point for infinite and semi-infinite array problems.

A major feature of wave scattering by periodic structures is the possibility of resonance effects. These effects were first observed in diffraction gratings experimentally by Wood [18] and partly explained theoretically by Rayleigh [19]. In the context of array scattering, occurrences of resonance are frequently referred to as Wood's anomalies [20]. Here, the waves scattered off each of the array's individual scatterers are in phase with each other and interfere constructively to form a plane wave propagating along the array.

A theoretical framework for resonance has been given for infinite arrays with Dirichlet and Neumann boundary conditions [21–27]. In these articles, Wood's anomalies were referred to as Rayleigh wavelengths and the scattered wave is considered as a monopole expansion ([25] is an exception on the latter). Linton & Thompson [28] studied the full multipole expansion in this setting, including solutions at single and double resonance. In the case of semi-infinite arrays, Millar [29] is (to the authors' knowledge) the only article that studies all possible types of single and double resonance. This article also recovered many results of [30], which exclusively specialized in the inward resonance case. Resonance has also been studied with finite [31,32] and circular arrays [33].

The uniqueness of the solution to the Helmholtz equation on an infinite domain with infinitely many scatterers is not *a priori* obvious and depends on the boundary conditions on the infinite scatterer [34,35]. In fact, the existence of Rayleigh–Bloch waves (modes that propagate along the grating and decay exponentially in orthogonal directions) can lead to non-uniqueness in certain circumstances (see [33,36–39]), though this can usually be eliminated by applying an appropriate periodicity condition [40]. In the present work, it is shown that non-uniqueness can also arise in problems where Rayleigh–Bloch surface waves do not exist.

Interesting phenomena, such as abnormal transmission or reflection, can often be observed around the resonant state [41,42]. Although a direct comparison is difficult due to the distinct geometry and approximations used in the studies, different smooth periodic boundaries and a grazing incidence can also lead to Wood's anomalies [43]. Homogenization techniques have also been employed to determine the effective properties of continuum models for wire meshes [44] and infinite arrays of penetrable scatterers [45,46], during which different kinds of resonances can occur.

This article considers resonance phenomena of two array scattering problems. The arrays are made of Dirichlet circular scatterers subject to Foldy's approximation [47]. Section 2 concentrates on resonance in the infinite array problem (figure 1*a*). Solutions at single and double resonance as well as the asymptotics in the double resonance limit are studied. A convenient method to illustrate non-uniqueness in this problem is also introduced. Section 3 will consider the semi-infinite array problem (figure 1*b*), including the outward resonance solution, some asymptotic approximations during inward resonance and the non-uniqueness during double resonance. In particular, a new and improved uniform far-field approximation is derived and implemented. Appendix A includes some asymptotic expansions for the Wiener–Hopf kernel that are vital for the results in §3, while appendix B considers the link between the semi-infinite array and the continuous half-plane. Appendix C gives a different perspective on the infinite array problem by not using Foldy's approximation and finds a unique solution in the double resonance limit.

For simplicity during the discussions here, we will position the arrays on the x-axis, with the semi-infinite array positioned on the positive side (figure 1). In other words, any formulae that we reuse from [17] will have the array angle set to zero (i.e. $\alpha = 0$). In these problems, the incident

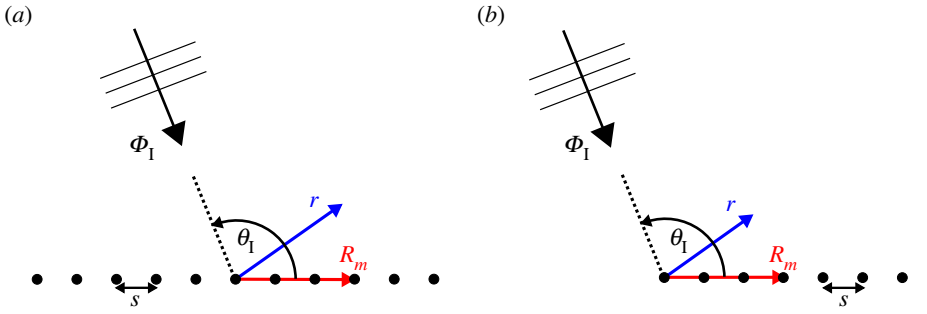

Figure 1. Diagrams of the (*a*) infinite and (*b*) semi-infinite arrays with the cylinders located at $\boldsymbol{R}_m$, the position vector $\boldsymbol{r}$ and the incident wave $\Phi_I = e^{-ikr\cos(\theta-\theta_I)}$. (Online version in colour.)

wave Φ_I will take the form of a plane wave with wavenumber k and incident angle θ_I (i.e. $\Phi_I = e^{-ikr\cos(\theta-\theta_I)}$) and the total field Φ will be required to satisfy Helmholtz's equation and Dirichlet boundary conditions.

To apply Foldy's approximation, we will need the radius of the scatterers a to be small in comparison to the incident wavelength (i.e. $ka \ll 1$). This approximation consists in assuming that the array scatterers are isotropic point scatterers. As a result, the scattered field ($\Phi_S = \Phi - \Phi_I$) is written in the form of a monopole expansion.

2. Infinite array problem

In the context of Foldy's approximation, the total field due to a plane wave incident on an infinite array of small circular scatterers with homogeneous Dirichlet boundary conditions [17] (figure 1*a*) can be expressed as

$$\Phi(\boldsymbol{r}) = \Phi_I(\boldsymbol{r}) + A_0^{(\inf)} \sum_{m=-\infty}^{\infty} e^{-iksm\cos(\theta_I)} H_0^{(1)}(k|\boldsymbol{r} - \boldsymbol{R}_m|). \tag{2.1}$$

Here, $H_0^{(1)}$ is the zeroth-order Hankel function of the first kind, the scatterers are located at $\boldsymbol{R}_m = ms\hat{\boldsymbol{x}}$, ($m \in \mathbb{Z}$) in a Cartesian basis ($\hat{\boldsymbol{x}}, \hat{\boldsymbol{y}}$) (figure 1) and

$$\begin{aligned} A_0^{(\inf)} &= -\frac{1}{K(e^{iks\cos(\theta_I)})} \\ &= -\left(H_0^{(1)}(ka) + 2\sum_{m=1}^{\infty} [\cos(ksm\cos(\theta_I)) H_0^{(1)}(ksm)] \right)^{-1}, \end{aligned} \tag{2.2}$$

where the kernel $K(z)$ is defined by (A 1). By using [48, eqn. (10.17.5)], we can determine the asymptotic behaviour of the sum end terms in (2.1) as $m \to \pm\infty$:

$$e^{-iksm\cos(\theta_I)} H_0^{(1)}(k|\boldsymbol{r} - \boldsymbol{R}_m|) \underset{m\to\pm\infty}{\sim} \sqrt{\frac{\pm 2}{\pi ksm}}\, e^{-iksm\cos(\theta_I)\pm iksm - ikr\cos(\theta) - (i\pi/4)}. \tag{2.3}$$

The form of (2.3) indicates that the total field summation (2.1) will fail to converge when $(ks/2\pi)(\pm 1 - \cos(\theta_I)) \in \mathbb{Z}$. At these points, the summation in (2.2) will also fail to converge and leads to $A_0^{(\inf)} \to 0$. However, this does not imply that the scattered field is zero. In fact, one can use the integral formula for the Hankel function and the Poisson summation formula to rewrite (2.1) as a sum of plane waves [15]

$$\Phi = \Phi_I + \frac{2A_0^{(\inf)}}{ks} \sum_{n=-\infty}^{\infty} \frac{e^{-ikr\cos(|\theta|+\psi_n)}}{\sin(\psi_n)}, \quad \theta \in (-\pi, \pi] \tag{2.4}$$

royalsocietypublishing.org/journal/rspa Proc. R. Soc. A 478: 20220604

where ψ_n (known as the scattering angles) are solutions to the equation

$$\cos(\psi_n) = \cos(\theta_\mathrm{I}) + \frac{2\pi}{ks} n. \tag{2.5}$$

The right-hand side of (2.5) is real for all parameter values. It is important to note that these scattering angles are defined such that $\mathrm{Re}\{\psi_n\} \in [0, \pi]$ and $\mathrm{Im}\{\sin(\psi_n)\} \geq 0$. This chosen branch means that each ψ_n is a point on one of three line segments on the complex plane.

— If $\cos(\theta_\mathrm{I}) + (2\pi/ks)n \in [-1, 1]$, then ψ_n is real and in $[0, \pi]$.
— If $\cos(\theta_\mathrm{I}) + (2\pi/ks)n > 1$, then $\psi_n = ix$, where $x > 0$.
— If $\cos(\theta_\mathrm{I}) + (2\pi/ks)n < -1$, then $\psi_n = \pi - ix$, where $x > 0$.

It should also be noted that these scattering angles differ from those of [15] by the identity $\psi_n = \pi - \psi_{-n}^{(\text{Linton and Martin})}$ due to a different incident angle $\theta_\mathrm{I} = \pi + \theta_\mathrm{I}^{(\text{Linton and Martin})}$. By using [49, eqns (8.522) and (8.524)], one can also rewrite (2.2) in terms of the scattering angles

$$A_0^{(\mathrm{inf})} = -\left[H_0^{(1)}(ka) - 1 - \frac{2\mathrm{i}}{\pi}\left(\gamma + \ln\frac{ks}{4\pi}\right) + \frac{2}{ks\sin(\psi_0)} + \sum_{\substack{n=-\infty \\ n\neq 0}}^{\infty} \left[\frac{2}{ks\sin(\psi_n)} + \frac{\mathrm{i}}{|n|\pi} \right] \right]^{-1}, \tag{2.6}$$

where $\gamma = 0.5772\cdots$ is the Euler–Mascheroni constant. With all this in mind, there are some distinctive interesting cases to consider.

Single resonance: If there exists a single integer $N \in \mathbb{Z}$ such that

— $\psi_N = 0$ and $N = (ks2\pi)(1 - \cos(\theta_\mathrm{I}))$ *or*
— $\psi_N = \pi$ and $N = (ks/2\pi)(-1 - \cos(\theta_\mathrm{I}))$

then single resonance occurs. In both cases, $\sin(\psi_N) \to 0$ which implies that

$$A_0^{(\mathrm{inf})} = -\left[\frac{2}{ks\sin(\psi_N)} + O(1) \right]^{-1}, \tag{2.7}$$

as $\psi_N \to 0$ or π. This simplifies the scattering angle formula for the total field (2.4) to

$$\Phi \underset{\psi_N \to 0,\pi}{\sim} \Phi_\mathrm{I} + \frac{2A_0^{(\mathrm{inf})}}{ks} \frac{\mathrm{e}^{-\mathrm{i}kr\cos(|\theta| + \psi_N)}}{\sin(\psi_N)}$$

and then the limit is taken to obtain

$$\Phi = \Phi_\mathrm{I} - \mathrm{e}^{\mp \mathrm{i}kr\cos(\theta)}, \tag{2.8}$$

where the upper (resp. lower) sign is for the case where $\psi_N = 0$ (resp. π). Due to (2.8), if $\theta_\mathrm{I} = 0$ or π, then the total field becomes identically zero (which is equivalent to the behaviour of an infinite plane with a homogeneous Dirichlet boundary condition). At $\boldsymbol{r} = \boldsymbol{R}_m$ (for any incident angle), we find that (2.8) satisfies the Dirichlet boundary conditions. As a result, the total fields will be almost zero on the cylinder surfaces (since the radius is small), therefore, the boundary conditions are satisfied in the limit of Foldy's approximation.

To reach resonance at non-grazing incidence (i.e. $\theta_\mathrm{I} \neq 0, \pi$), it is necessary to have non-zero N and $ks \geq \pi$. Though in this case ks is at least $O(1)$, it is not incompatible with the validity of Foldy's approximation. Indeed, this approximation remains valid if we assume that $a \ll s$ (i.e. wide spacing between the scatterers). For this reason, it makes sense to talk about resonance phenomena in the context of Foldy's approximation. This comment remains true for all other resonance phenomena considered in this article.

Double resonance: If both resonance conditions are satisfied at the same time (i.e. $(ks/2\pi)(1 - \cos(\theta_\mathrm{I})) \in \mathbb{Z}$ and $(ks/2\pi)(-1 - \cos(\theta_\mathrm{I})) \in \mathbb{Z}$), then double resonance occurs. Note that in this

problem and the semi-infinite array problem, this is the maximum number of resonances that can occur simultaneously. Double resonance results in the scattered field comprising of two resonant waves instead of one. With this in mind, we pose the following ansatz,

$$\Phi = \Phi_{\mathrm{I}} + c_1\,\mathrm{e}^{-\mathrm{i}kr\cos(\theta)} + c_2\,\mathrm{e}^{\mathrm{i}kr\cos(\theta)}. \tag{2.9}$$

Applying the Dirichlet boundary conditions at $\boldsymbol{r} = \boldsymbol{R}_n$ to (2.9) gives us a condition for the amplitudes; $1 + c_1 + c_2 = 0$. However, to obtain a unique solution, we need a second condition for c_1 and c_2. This second condition cannot be obtained if we only consider monopole terms (i.e. $H_0^{(1)}$), which means that Foldy's approximation fails to give a unique solution in the case of double resonance. Notably, this non-uniqueness does not occur if full linear multiple scattering theory is applied (see appendix C). Retaining monopoles and dipoles (as opposed to monopoles only as in (2.1)) leads to the result $\cos(\theta_{\mathrm{I}}) + c_1 - c_2 = 0$ (C 20), so the correct expression for the total field is

$$\Phi = \Phi_{\mathrm{I}} - \cos^2\left(\frac{\theta_{\mathrm{I}}}{2}\right)\mathrm{e}^{-\mathrm{i}kr\cos(\theta)} - \sin^2\left(\frac{\theta_{\mathrm{I}}}{2}\right)\mathrm{e}^{\mathrm{i}kr\cos(\theta)}. \tag{2.10}$$

Setting $\theta_{\mathrm{I}} = 0$ or π leads to a solution equivalent to equation (37) in [28] where the scattered field cancels out the incident wave to result in a zero total field.

Within Foldy's approximation, i.e. we only consider monopole terms, we can explicitly exhibit the resulting non-uniqueness by considering different ways of approaching double resonance. Indeed during double resonance, there exist two integers $N_\pm$ such that $\psi_{N_+} = 0$ and $\psi_{N_-} = \pi$ and this can only happen if ks is a multiple of π (in fact, we can write $ks = (N_+ - N_-)\pi$ and $\cos(\theta_{\mathrm{I}}) = (N_+ + N_-)/(N_+ - N_-)$). Note that $N_+ = (ks/2\pi)[1 - \cos(\theta_{\mathrm{I}})] \geq 0$ and $N_- = (ks/2\pi)[-1 - \cos(\theta_{\mathrm{I}})] \leq 0$. Since there are only two resonance conditions here, there is no case where we have three or more integers satisfying the conditions at the same time. Determining the double resonance solution requires us to balance two limits $\psi_{N_+} \to 0$ and $\psi_{N_-} \to \pi$. With this in mind, the coefficient $A_0^{(\mathrm{inf})}$ reduces to

$$A_0^{(\mathrm{inf})} = -\left[\frac{2}{ks\sin(\psi_{N_+})} + \frac{2}{ks\sin(\psi_{N_-})} + O(1)\right]^{-1}, \tag{2.11}$$

and then (2.4) reduces to

$$\begin{aligned}\Phi &\sim \Phi_{\mathrm{I}} + \frac{2A_0^{(\mathrm{inf})}}{ks}\left[\frac{\mathrm{e}^{-\mathrm{i}kr\cos(\theta)}}{\sin(\psi_{N_+})} + \frac{\mathrm{e}^{\mathrm{i}kr\cos(\theta)}}{\sin(\psi_{N_-})}\right],\\ &\sim \Phi_{\mathrm{I}} - \frac{1}{1+\beta}\mathrm{e}^{-\mathrm{i}kr\cos(\theta)} - \frac{1}{1+\beta^{-1}}\,\mathrm{e}^{\mathrm{i}kr\cos(\theta)},\end{aligned} \tag{2.12}$$

where $\beta \sim (\sin(\psi_{N_+})/\sin(\psi_{N_-}))$ as $\psi_{N_+} \to 0$ and $\psi_{N_-} \to \pi$. Finding the limit of β is not a trivial task and requires one to know how $\sin(\psi_{N_+}) \to 0$ in relation to $\sin(\psi_{N_-}) \to 0$. In order to obtain this information, one needs to determine the asymptotic behaviour of $\sin(\psi_{N_\pm})$ when approaching double resonance. Some different possibilities of solutions are presented in (2.17)–(2.20). While we could approach this by determining the asymptotic behaviour of $\psi_{N_\pm}$, this is largely unnecessary. Instead, we consider the relation $\sin(z) = \mathrm{i}\sqrt{-\mathrm{i}(1-\cos(z))}\sqrt{-\mathrm{i}(1+\cos(z))}$, where the square roots take the principal branch. Then β is simplified to

$$\beta \sim \frac{\sqrt{-\mathrm{i}(1-\cos(\psi_{N_+}))}\sqrt{-\mathrm{i}(1+\cos(\psi_{N_+}))}}{\sqrt{-\mathrm{i}(1-\cos(\psi_{N_-}))}\sqrt{-\mathrm{i}(1+\cos(\psi_{N_-}))}} \sim \frac{\sqrt{-\mathrm{i}(1-\cos(\psi_{N_+}))}}{\sqrt{-\mathrm{i}(1+\cos(\psi_{N_-}))}}, \tag{2.13}$$

because the top right and bottom left square roots are well-behaved and evaluate to $2\,\mathrm{e}^{-(\mathrm{i}\pi/4)}$ as $\psi_{N_+} \to 0$ and $\psi_{N_-} \to \pi$, respectively.

Let us assume that k, s and θ_{I} take values such that $\cos(\theta_{\mathrm{I}}) + (2\pi/ks)N_\pm = \pm 1$ and define two perturbations $d_1\epsilon$ and $d_2\epsilon$ in terms of a small parameter $0 \leq \epsilon \ll 1$ and two complex constants d_1

and d_2 indicating the direction of the perturbation. We then take (2.5) and replace θ_I with $\theta_\mathrm{I} + d_1\epsilon$ and replace k with $k(1 + d_2\epsilon)$ to obtain

$$\cos(\psi_{N_\pm}) = \cos(\theta_\mathrm{I} + d_1\epsilon) + \frac{2\pi N_\pm}{ks(1 + d_2\epsilon)}. \tag{2.14}$$

We expand (2.14) as $\epsilon \to 0$ using the Taylor expansions $\cos(\theta_\mathrm{I} + d_1\epsilon) = \cos(\theta_\mathrm{I}) - d_1\epsilon \sin(\theta_\mathrm{I}) + O(\epsilon^2)$ and $(1 + d_2\epsilon)^{-1} = 1 - d_2\epsilon + O(\epsilon^2)$ to give

$$\begin{aligned}\cos(\psi_{N_\pm}) &= \cos(\theta_\mathrm{I}) - d_1\epsilon \sin(\theta_\mathrm{I}) + \frac{2\pi N_\pm}{ks}(1 - d_2\epsilon) + O(\epsilon^2),\\ &= \pm\Big(1 - (\pm d_1 \sin(\theta_\mathrm{I}) + d_2(1 \mp \cos(\theta_\mathrm{I})))\epsilon + O(\epsilon^2)\Big).\end{aligned} \tag{2.15}$$

Then we substitute (2.15) into (2.13) which becomes

$$\beta \sim \frac{\sqrt{-\mathrm{i}(d_1 \sin(\theta_\mathrm{I}) + d_2(1 - \cos(\theta_\mathrm{I})))}}{\sqrt{\mathrm{i}(d_1 \sin(\theta_\mathrm{I}) - d_2(1 + \cos(\theta_\mathrm{I})))}}. \tag{2.16}$$

This solution leads to infinitely many different possible solutions. In particular, it is possible to recover all the following solutions with certain special choices of d_1 and d_2.

— If $d_2 = 0$ and $d_1 \sin(\theta_\mathrm{I}) > 0$ then $\beta = -i$, which implies that,

$$\Phi = \Phi_\mathrm{I} - \frac{1 + \mathrm{i}}{2}\,\mathrm{e}^{-\mathrm{i}kr\cos(\theta)} - \frac{1 - \mathrm{i}}{2}\,\mathrm{e}^{\mathrm{i}kr\cos(\theta)}. \tag{2.17}$$

— If $d_2 = 0$ and $d_1 \sin(\theta_\mathrm{I}) < 0$ then $\beta = i$, which implies that,

$$\Phi = \Phi_\mathrm{I} - \frac{1 - \mathrm{i}}{2}\,\mathrm{e}^{-\mathrm{i}kr\cos(\theta)} - \frac{1 + \mathrm{i}}{2}\,\mathrm{e}^{\mathrm{i}kr\cos(\theta)}. \tag{2.18}$$

— If $d_1 = 0$ then $\beta = \sqrt{(1 - \cos(\theta_\mathrm{I}))/(1 + \cos(\theta_\mathrm{I}))} = |\tan(\theta_\mathrm{I}/2)|$, which implies that,

$$\Phi = \Phi_\mathrm{I} - \frac{1}{1 + \left|\tan\left(\frac{\theta_\mathrm{I}}{2}\right)\right|}\,\mathrm{e}^{-\mathrm{i}kr\cos(\theta)} - \frac{1}{1 + |\cot(\theta_\mathrm{I}/2)|}\,\mathrm{e}^{\mathrm{i}kr\cos(\theta)}. \tag{2.19}$$

— If $d_1 = \sin(\theta_\mathrm{I})\cos(\theta_\mathrm{I})$ and $d_2 = -(1 + \cos^2(\theta_\mathrm{I}))$ then $\beta = (1 - \cos(\theta_\mathrm{I}))/(1 + \cos(\theta_\mathrm{I})) = \tan^2(\theta_\mathrm{I}/2)$, leading to

$$\Phi = \Phi_\mathrm{I} - \cos^2\left(\frac{\theta_\mathrm{I}}{2}\right)\mathrm{e}^{-\mathrm{i}kr\cos(\theta)} - \sin^2\left(\frac{\theta_\mathrm{I}}{2}\right)\mathrm{e}^{\mathrm{i}kr\cos(\theta)}. \tag{2.20}$$

The first three solutions were given by Millar [26] who was the first to suggest such non-uniqueness. The last solution recovers the solution from [28] given by (2.10).

(a) Visualizing uniqueness/non-uniqueness

In this section, we show a way to visualize uniqueness and non-uniqueness in this context. To do this, we replace θ_I and k with the perturbations $\theta_\mathrm{I} + d_1\epsilon$ and $k(1 + d_2\epsilon)$ in the wave field (2.4). For uniqueness, it is required that $\Phi(r, \theta; k(1 + d_2\epsilon), \theta_\mathrm{I} + d_1\epsilon)$ tends to the same limit for all values of d_1 and d_2 as $\epsilon \to 0^+$. Let us define the reference limit $\Phi_{(\mathrm{limit})} = \lim_{\epsilon\to 0^+} \Phi(r, \theta; k, \theta_\mathrm{I} + \epsilon)$ and then for simplicity, use the parameterization $d_1 = \cos(\sigma)$ and $d_2 = \sin(\sigma)$ where $\sigma \in (-\pi, \pi]$. Then, we evaluate the error function $|\Phi(r, \theta; k(1 + \epsilon \sin(\sigma)), \theta_\mathrm{I} + \epsilon \cos(\sigma)) - \Phi_{(\mathrm{limit})}|$ with respect to σ (at a fixed position (r, θ)) and as $\epsilon \to 0^+$. The idea is that if the value of $\Phi(r, \theta; k, \theta_\mathrm{I})$ is unique then the error converges to zero for all σ. However, if there exists a σ such that the error does not converge to zero then $\Phi(r, \theta; k, \theta_\mathrm{I})$ is not unique. It is clear that comparing the wave field (2.4) with the given limits (2.8) and (2.12) will highlight the uniqueness of the single resonance case and the non-uniqueness of the double resonance case in the infinite array problem.

Figure 2 visualizes this error function by displaying some heat maps with respect to σ where each bar corresponds to a fixed value of ϵ. It includes a non-resonant case (*a*) with a unique

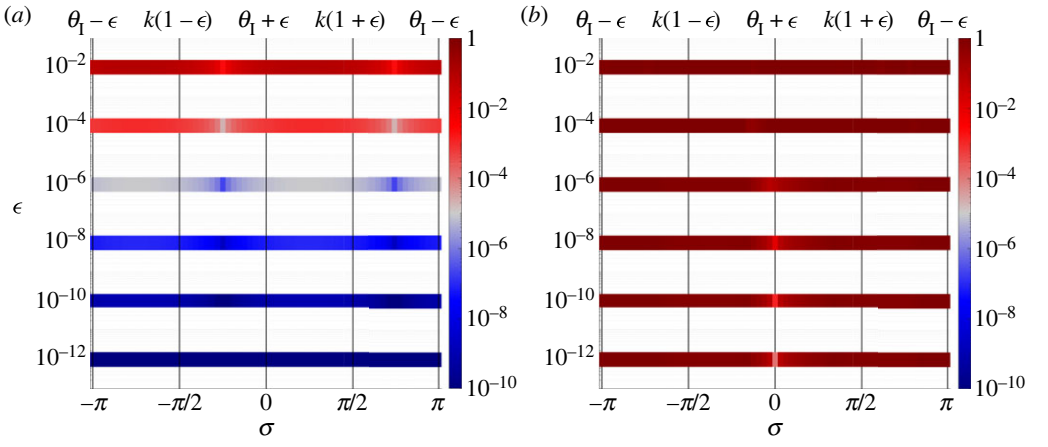

Figure 2. Visualization of the wave field uniqueness for the infinite array problem using (2.4) at $(r, \theta) = (10s, \pi/4)$, where $s = 0.1$ and $a = 0.001$. (*a*) A non-resonant case, which has a unique limit, where $k = 40\pi/3$ and $\theta_I = \pi/2$. (*b*) A double resonance case, which does not have a unique limit, where $k = 40\pi$ and $\theta_I = 2\pi/3$. (Online version in colour.)

limit and a double resonance case (*b*) with a non-unique limit. Figure 8*a* is a graph plotting the bar's average with respect to ϵ. This includes two non-resonant cases as well as single and double resonance. We see here that cases with a unique limit show convergence as $\epsilon \to 0^+$. Among these is the single resonance case, which converges slower than non-resonance and may suffer numerical error issues as ϵ becomes smaller. Although observations from these particular plots are already known to us from earlier in this article, we have introduced the concept of this visualization for the infinite array, because we intend to use it later for the less conclusive semi-infinite array.

3. Semi-infinite array problem

Now we will examine the different resonant cases in the more interesting and less studied setting of a semi-infinite array. Recall the scattered field solution (figure 1*b*) given by (2.2) and (2.22) of [17] which was found via the discrete Wiener–Hopf technique,

$$\Phi_S(\boldsymbol{r}) = \sum_{m=0}^{\infty} [A_m^{(\text{s-inf})} H_0^{(1)}(k|\boldsymbol{r} - \boldsymbol{R}_m|)],$$

$$\text{where } A_m^{(\text{s-inf})} = -\sum_{n=0}^{m} \left[\frac{\lambda_n \, \mathrm{e}^{-\mathrm{i}ks(m-n)\cos(\theta_I)}}{K^+(\mathrm{e}^{-\mathrm{i}ks\cos(\theta_I)})} \right]. \tag{3.1}$$

Here, we reuse the definitions of the discrete Wiener–Hopf kernel (A 2), its factors (A 5) and the coefficients

$$\lambda_n = \frac{1}{n!} \frac{\mathrm{d}^n}{\mathrm{d}z^n} \left[\frac{1}{K^+(z)} \right]_{z=0}$$

from [17]. We can rewrite (3.1) in integral form as explained in §3.3 of [14]. Hence,

$$\Phi_S(r, \theta) = \frac{1}{\pi K^+(\mathrm{e}^{-\mathrm{i}ks\cos(\theta_I)})} \int_{\pi - \mathrm{i}\infty}^{\mathrm{i}\infty} \frac{\mathrm{e}^{\mathrm{i}kr\cos(|\theta| - \varphi)}}{K^-(\mathrm{e}^{\mathrm{i}ks\cos(\varphi)})(1 - \mathrm{e}^{-\mathrm{i}ks(\cos(\varphi) + \cos(\theta_I))})} \mathrm{d}\varphi. \tag{3.2}$$

The integration contour is a series of three straight lines from $\pi - \mathrm{i}\infty$ to $\mathrm{i}\infty$ via the waypoints π and 0. The integrand has an infinite number of poles and branchcuts, from which the contour is indented above and to the right of. The branchcuts start at $\varphi_n^{(\text{bp})} = \cos^{-1}((2\pi n/ks) + 1)$ and follow

the curved path given by $\varphi = \cos^{-1}(\cos(\varphi_n^{(\mathrm{bp})}) + it)$ from $t = 0$ to ∞. The poles are simple and located at $\varphi_n^{(\mathrm{pole})} = \cos^{-1}((2\pi n/ks) - \cos(\theta_\mathrm{I}))$ and have associated residues,

$$\frac{\mathrm{i}\,\mathrm{e}^{\mathrm{i}kr\cos(|\theta|-\varphi_n^{(\mathrm{pole})})}}{\pi ksK(\mathrm{e}^{-\mathrm{i}ks\cos(\theta_\mathrm{I})})\sin(\varphi_n^{(\mathrm{pole})})}. \tag{3.3}$$

Hills & Karp [14] used this integral to create a far-field approximation for the scattered field. After deforming to the steepest descent contour, the end result is a summation of the residues (3.3) where $|\theta| < \varphi_n^{(\mathrm{pole})} < \pi$ is real, plus a cylindrical wave contribution from the saddle point at $|\theta|$. They neglect integral contributions from branch cuts, explaining that these are higher-order terms in most cases. Their final result is the following far-field ($kr \to \infty$) approximation,

$$\begin{aligned}\Phi_S(r,\theta) \underset{kr\to\infty}{=} &- \sum_{\substack{\varphi_n^{(\mathrm{pole})}\in\mathbb{R} \\ \varphi_n^{(\mathrm{pole})}>|\theta|}} \frac{2\,\mathrm{e}^{\mathrm{i}kr\cos(|\theta|-\varphi_n^{(\mathrm{pole})})}}{ksK(\mathrm{e}^{-\mathrm{i}ks\cos(\theta_\mathrm{I})})\sin(\varphi_n^{(\mathrm{pole})})} \\ &- \frac{\sqrt{(2/\pi kr)}\,\mathrm{e}^{\mathrm{i}kr-(\mathrm{i}\pi/4)}}{K^+(\mathrm{e}^{-\mathrm{i}ks\cos(\theta_\mathrm{I})})K^-(\mathrm{e}^{\mathrm{i}ks\cos(\theta)})(1-\mathrm{e}^{-\mathrm{i}ks(\cos(\theta)+\cos(\theta_\mathrm{I}))})} + o((kr)^{-(1/2)}).\end{aligned} \tag{3.4}$$

The conditions for resonance in the semi-infinite array problem remain the same as the infinite array problem; $((ks/2\pi)(1 \pm \cos(\theta_\mathrm{I})) \in \mathbb{Z})$. However, the two conditions lead to two different types of single resonance, which [14] refers to as outward and inward.

Outward resonance: Satisfying the condition $(ks/2\pi)(1 - \cos(\theta_\mathrm{I})) \in \mathbb{Z}$, outward resonance is very similar to the behaviour of resonant waves in the infinite array problem. In this case, the scattering coefficients $A_n^{(\text{s-inf})}$ tend to zero because the factor $K^+(\mathrm{e}^{-\mathrm{i}ks\cos(\theta_\mathrm{I})})$ in (3.1) is singular. However, the scattered wave field is not zero. Contributions to the integral in (3.2) tend to zero, except for the residue from one pole, located at $\varphi_n^{(\mathrm{pole})} = \pi$. This residue is non-zero because $\sin(\varphi_n^{(\mathrm{pole})}) \to 0$ at the same rate as $K(\mathrm{e}^{-\mathrm{i}ks\cos(\theta_\mathrm{I})}) \to \infty$, which leads to the total field being no different to (2.8)

$$\Phi = \mathrm{e}^{-\mathrm{i}kr\cos(\theta-\theta_\mathrm{I})} - \mathrm{e}^{-\mathrm{i}kr\cos(\theta)}. \tag{3.5}$$

This was also the conclusion of [14,29]. Interestingly, if we were to evaluate $A_n^{(\text{s-inf})}$ using the approximate Wiener–Hopf kernel (see appendix A.3 of [17] for details), we would incorrectly obtain non-zero scattering coefficients due to the approximate kernel being finite at the branch points. Despite this, the Hankel summation given by (3.1) still numerically yields plane wave-like behaviour for the resonant scattered field (this is illustrated in figure 3*a*) but with an amplitude that depends on the truncation value M. We can show this if we take the Hankel summation (3.1) with the sum terms replaced by their asymptotic expansions as $m \to \infty$,

$$\sum_{m=0}^{M}[A_m^{(\text{s-inf})}\,H_0^{(1)}(k|\boldsymbol{r}-\boldsymbol{R}_m|)] \sim \sqrt{\frac{2}{\pi ks}}\frac{\mathrm{e}^{-\mathrm{i}kr\cos(\theta)+(3\pi\mathrm{i}/4)}}{\widetilde{K}(\mathrm{e}^{\mathrm{i}ks\cos(\theta_\mathrm{I})})}\sum_{m=0}^{M} m^{-(1/2)}, \tag{3.6}$$

where $\widetilde{K}$ represents the approximate kernel. In (3.6), we have a plane wave factor which explains the behaviour in figure 3*a*. The sum $\sum_{m=0}^{M} m^{-\frac{1}{2}}$ is $O(M^{1/2})$ as $M \to \infty$ which implies that the numerical amplitude is also of the same order. We show this behaviour in figure 3*b* where we plotted the numerical amplitude's absolute value (simulated from (3.1) by the quantity $|\Phi_S(0.1, \pi/2)|$) against M and then compared it with the true amplitude.

Inward resonance: The behaviour of the total field during inward resonance (when $(ks/2\pi)(1 + \cos(\theta_\mathrm{I})) \in \mathbb{Z}$) is quite different from the behaviour during outward resonance because the scattering coefficients are now non-zero. In fact, the scattering coefficients have the asymptotic behaviour given by $A_n^{(\text{s-inf})} = O(\mathrm{e}^{\mathrm{i}ksn}n^{-(1/2)})$ as $n \to \infty$ which decays faster than in the non-resonant cases. This means that we do not have the same numerical issues related to the truncation value as we did for the outward resonance case. The resulting inward resonance wave starts at the

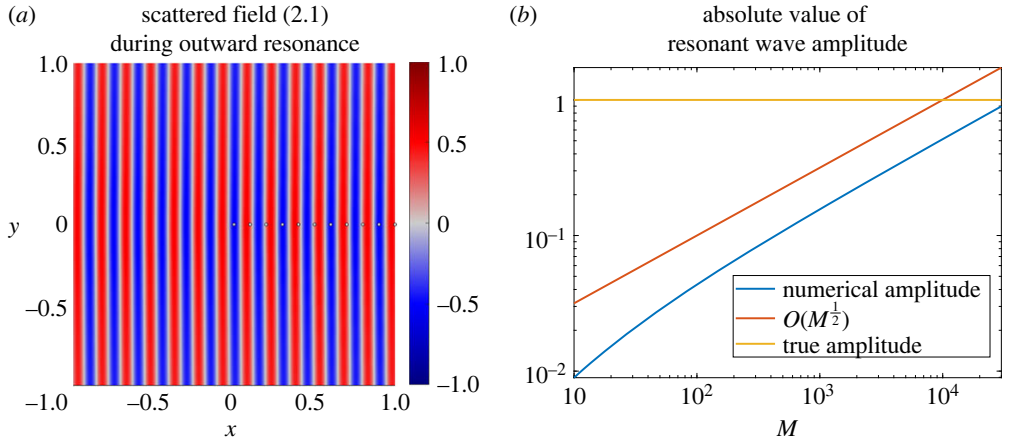

Figure 3. (*a*) The real part of an outward resonance example of the Hankel summation solution (3.1) (where the truncation is at $M = 10\,000$) using the approximate Wiener–Hopf kernel. The right side plots the absolute value of the numerical resonant wave amplitude with respect to the truncation M. (*b*) The behaviour of the numerical amplitude as $M \to \infty$ and compares it with the true amplitude. Here, the incident wave is defined by the parameters $k = 40\pi/3$ and $\theta_{\mathrm{I}} = 2\pi/3$ and the scatterers of the semi-infinite array are positioned on the positive x-axis with radius $a = 0.001$ and spacing $s = 0.1$. (Online version in colour.)

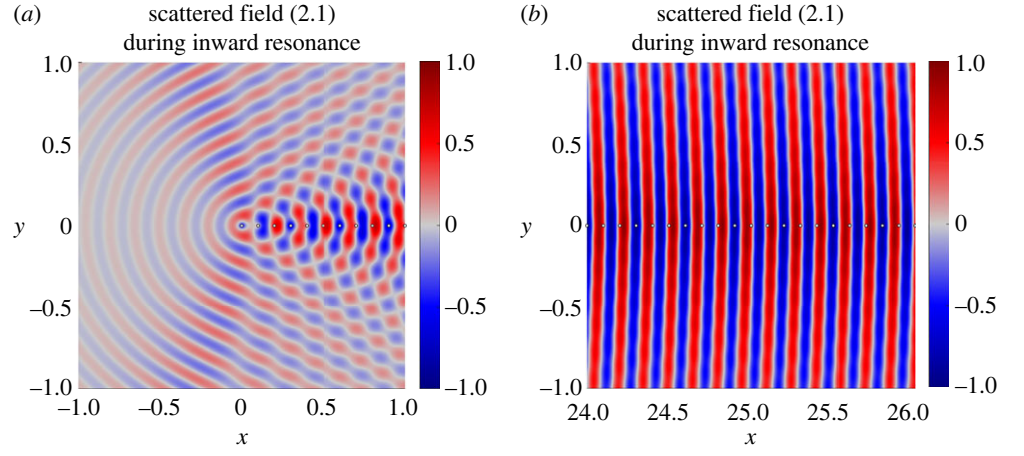

Figure 4. Real part of the scattered field associated with the inward resonance example of the Hankel summation solution (3.1) (where the truncation is at $M = 10\,000$) visualized around the origin (*a*) and further down the array (*b*). Here, the incident wave is defined by the parameters $k = 40\pi/3$ and $\theta_{\mathrm{I}} = \pi/3$ and the scatterers of the semi-infinite array are positioned on the positive x-axis with radius $a = 0.001$ and spacing $s = 0.1$. (Online version in colour.)

edge of the array as a cylindrical wave supported within an angular region and slowly interferes with other scattered waves to become a full plane wave at infinity (figure 4).

Dedicated to this special case, the article [30] looks into the far-field asymptotics of (3.2) and deduces numerous asymptotic formulae valid for different regions of θ assuming that kr is sufficiently large. Since we now have $\cos(\theta_{\mathrm{I}}) = (2\pi/ks)m - 1$ for some integer m, the location of the pole with index $n + m$ coincides with the branch point with index n, i.e. $\varphi_{n+m}^{(\mathrm{pole})} = \varphi_n^{(\mathrm{bp})} = \varphi_n = \cos^{-1}((2\pi n/ks) + 1)$. This means that the previously neglected branch cut contributions can no longer be ignored. As a consequence, the pole-residue sum in the far-field approximation (3.4)

is no longer valid. Instead, the new far-field approximation (when $|\theta| \neq \varphi_n$) is a summation of combined pole and branch cut contributions as well as the original saddle point contribution,

$$\Phi_S \approx -\frac{\sqrt{(2/\pi kr)}\,\mathrm{e}^{\mathrm{i}kr-(\mathrm{i}\pi/4)}}{K^+(\mathrm{e}^{-\mathrm{i}ks\cos(\theta_\mathrm{I})})K^-(\mathrm{e}^{\mathrm{i}ks\cos(\theta)})(1-\mathrm{e}^{-\mathrm{i}ks(\cos(\theta)+\cos(\theta_\mathrm{I}))})} + \sum_{\substack{\varphi_n\in\mathbb{R}\\ \varphi_n>|\theta|}} \frac{1}{\pi K^+(\mathrm{e}^{-\mathrm{i}ks\cos(\theta_\mathrm{I})})} \fint \frac{\mathrm{e}^{\mathrm{i}kr\cos(|\theta|-\varphi)}}{K^-(\mathrm{e}^{\mathrm{i}ks\cos(\varphi)})(1-\mathrm{e}^{-\mathrm{i}ks(\cos(\varphi)+\cos(\theta_\mathrm{I}))})}\,\mathrm{d}\varphi. \tag{3.7}$$

Here, $\fint$ represents an integral around the branch cut starting at the branch point $\varphi=\varphi_n$ where $|\theta|<\varphi_n<\pi$ (figure 5). Note that during inward resonance, we have $\mathrm{e}^{-\mathrm{i}ks\cos(\theta_\mathrm{I})}=\mathrm{e}^{\mathrm{i}ks}$ which removes the θ_I dependency entirely from the scattered field. This means that, for fixed k, a and s, every case of inward resonance has exactly the same Φ_S. However, if we were using the full multipole expansion, the scattered field at every inward resonance is composed of a constant (equal to 1 within Foldy's approximation) multiplied by the scattered field at head-on incidence $\theta_\mathrm{I}=\pi$, plus some extra terms (which disappear with Foldy's approximation). Equation (3.7) is now simplified to

$$\Phi_S \approx -I(\theta)\sqrt{\frac{2}{\pi kr}}\,\mathrm{e}^{\mathrm{i}kr-(\mathrm{i}\pi/4)} + \sum_{\substack{\varphi_n\in\mathbb{R}\\ \varphi_n>|\theta|}} \frac{1}{\pi} \fint I(\varphi)\,\mathrm{e}^{\mathrm{i}kr\cos(|\theta|-\varphi)}\,\mathrm{d}\varphi,$$

where

$$I(\varphi)=\frac{1}{K^+(\mathrm{e}^{\mathrm{i}ks})K^-(\mathrm{e}^{\mathrm{i}ks\cos(\varphi)})(1-\mathrm{e}^{\mathrm{i}ks(1-\cos(\varphi))})}. \tag{3.8}$$

To evaluate $\fint$, we start by expanding the integrand about $\varphi=\varphi_n$. We do this by using $K^-(z)=K^+(1/z)$, (A 6) and some elementary algebra, which leads to

$$I(\varphi)\sim \frac{\mathrm{e}^{(\mathrm{i}\pi/4)}}{\sqrt{-2\mathrm{i}(\cos(\varphi_n)-\cos(\varphi))}} \times \left(\frac{1}{\begin{array}{c}1+((1+\mathrm{i})/2)ks\mathcal{K}_1\sqrt{-\mathrm{i}(\cos(\varphi_n)-\cos(\varphi))}-\mathrm{i}\mathcal{K}_2(\cos(\varphi_n)-\cos(\varphi))\\ +O((-\mathrm{i}(\cos(\varphi_n)-\cos(\varphi)))^{(3/2)})\end{array}}\right), \tag{3.9}$$

where $\mathcal{K}_1$ is given by (A 4),

$$\mathcal{K}_2=\frac{\mathrm{i}}{4}-\frac{ks}{2}-ks\,\mathrm{e}^{\mathrm{i}ks}\frac{K^{+'}(\mathrm{e}^{\mathrm{i}ks})}{K^+(\mathrm{e}^{\mathrm{i}ks})}, \tag{3.10}$$

and $K^{+'}(\mathrm{e}^{\mathrm{i}ks})/K^+(\mathrm{e}^{\mathrm{i}ks})$ is given by (A 7). We can simplify (3.9) further by noting that, $\cos(\varphi_n)-\cos(\varphi)\approx\sin(\varphi_n)(\varphi-\varphi_n)$ when $\varphi\approx\varphi_n$.

We split $\fint$ into three parts with three parameterizations; Γ_1, Γ_2 and Γ_3 (figure 5) which are given by,

$$\Gamma_1=\{\varphi|\varphi=\varphi_n+t\,\mathrm{e}^{-(\mathrm{i}\pi/2)},\varepsilon\le t\le\eta\},$$

$$\Gamma_2=\left\{\varphi|\varphi=\varphi_n+\epsilon\,\mathrm{e}^{\mathrm{i}t},-\frac{\pi}{2}\le t\le\frac{3\pi}{2}\right\}$$

and

$$\Gamma_3=\{\varphi|\varphi=\varphi_n+t\,\mathrm{e}^{3\pi i/2},\varepsilon\le t\le\eta\},$$

where $0<\varepsilon<\eta$ and $\varepsilon\ll1$. The integral over Γ_2 is of the order $O(\sqrt{\varepsilon})$ as $\varepsilon\to0$, so it tends to zero in the limit. The other parts are two sides of the same branch cut which can be pieced together to

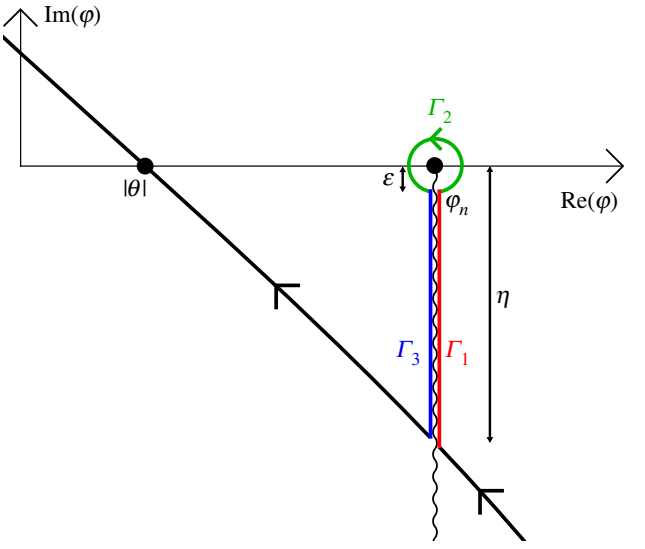

Figure 5. An illustration of the contour around the branch point φ_n for $\oint$ as the sum of its parts $\int_{\Gamma_1}, \int_{\Gamma_2}$ and $\int_{\Gamma_3}$ which depend on the parameters ε and η. Note that the black line is a segment of the steepest descent contour through the saddle point $|\theta|$. (Online version in colour.)

obtain

$$\frac{1}{\pi}\oint I(\varphi)\,\mathrm{e}^{\mathrm{i}kr\cos(|\theta|-\varphi)}\,\mathrm{d}t \approx -\frac{(1+\mathrm{i})}{\pi\sqrt{\sin(\varphi_n)}}\int_0^{\eta}\frac{(1-\mathcal{K}_2 t)\,\mathrm{e}^{\mathrm{i}kr\cos(|\theta|-\varphi_n+\mathrm{i}t)}}{\sqrt{t}(1+((\mathrm{i}(ks\mathcal{K}_1)^2/2)-2\mathcal{K}_2)t)}\,\mathrm{d}t. \tag{3.11}$$

We can expand the non-exponential part of the integrand for small t but this is only valid if $\eta < |2/(\mathrm{i}(ks\mathcal{K}_1)^2 - 4\mathcal{K}_2)|$. For now, we shall assume that it is valid then,

$$\frac{1}{\pi}\oint I(\varphi)\,\mathrm{e}^{\mathrm{i}kr\cos(|\theta|-\varphi)}\mathrm{d}t \approx -\frac{(1+\mathrm{i})}{\pi\sqrt{\sin(\varphi_n)}}\int_0^{\eta}\frac{\mathrm{e}^{\mathrm{i}kr\cos(|\theta|-\varphi_n+\mathrm{i}t)}}{\sqrt{t}}\,\mathrm{d}t. \tag{3.12}$$

After expanding the exponent for small t, the result can be written in terms of the error function, which is approximated for large argument (specifically $kr\eta \gg 1$). Then we obtain the final approximation

$$\frac{1}{\pi}\oint I(\varphi)\,\mathrm{e}^{\mathrm{i}kr\cos(|\theta|-\varphi)}\mathrm{d}\varphi \approx -\frac{(1+\mathrm{i})\,\mathrm{e}^{\mathrm{i}kr\cos(|\theta|-\varphi_n)}}{\sqrt{\pi kr\sin(\varphi_n)\sin(\varphi_n-|\theta|)}}. \tag{3.13}$$

If the condition $\eta < |2/(\mathrm{i}(ks\mathcal{K}_1)^2 - 4\mathcal{K}_2)|$ is not true, then we split the integral into two parts $\int_0^{\eta} = \int_0^{\hat{\eta}} + \int_{\hat{\eta}}^{\eta}$ where $\hat{\eta}$ is such that $(1/kr) \ll \hat{\eta} < |2/(\mathrm{i}(ks\mathcal{K}_1)^2 - 4\mathcal{K}_2)|$. The first part is approximated as before, which leads to (3.13). The absolute value of the second part has an upper bound of the order $O(\mathrm{e}^{-kr\sin(\varphi_n-|\theta|)\sinh(\hat{\eta})})$, which is exponentially small for large kr. This means that the second part can be neglected completely. Hence, the far-field approximation during inward resonance is given by

$$\Phi_S \approx -I(\theta)\sqrt{\frac{2}{\pi kr}}\,\mathrm{e}^{\mathrm{i}kr-\frac{\mathrm{i}\pi}{4}} - \sum_{\substack{\varphi_n\in\mathbb{R}\\ \varphi_n>|\theta|}}\frac{(1+\mathrm{i})\,\mathrm{e}^{\mathrm{i}kr\cos(|\theta|-\varphi_n)}}{\sqrt{\pi kr\sin(\varphi_n)\sin(\varphi_n-|\theta|)}}. \tag{3.14}$$

We compare this new far-field approximation with the Hankel summation in figure 6. This plot reasserts that this far-field approximation works very well provided kr is large and $|\theta| \neq \varphi_n$.

Even though the far-field approximation is invalid when $|\theta| \approx \varphi_n$, it is still possible to obtain *uniform* far-field approximations that are valid in those regions. In these cases, the saddle point

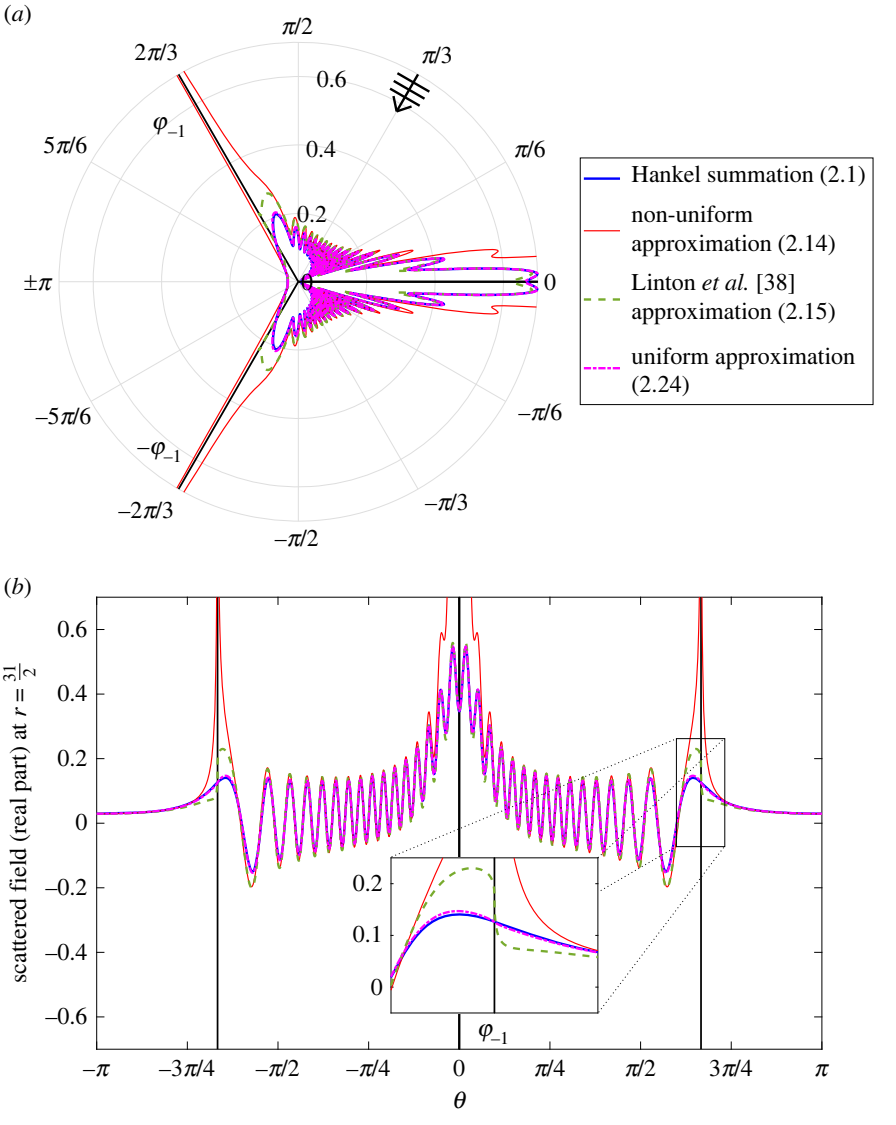

Figure 6. Plots of the Hankel summation (where the truncation is at $M = 10\,000$) compared with the non-uniform (3.14) and uniform far-field approximations, as well as the approximation given by (3.15) from [38]. Here, the top (bottom) side compares the absolute value (real part). In these plots, we have $r = 31s/2$, the incident wave is defined by the parameters $k = 40\pi/3$ and $\theta_{\mathrm{I}} = \pi/3$ and the semi-infinite array is defined by $a = 0.001$ and $s = 0.1$. The black lines indicate locations of $\pm\varphi_n$. (Online version in colour.)

collides with the branch point at φ_n, meaning that the saddle point contribution needs to be reworked. Linton *et al.* [38] were able to find two far-field approximations (one non-uniform and one uniform in θ) during inward resonance without using Foldy's approximation. Their non-uniform formula (given by equation (5.11)) matches our version (3.14) after applying Foldy's approximation, which is done by discarding all non-zero n terms in equations (5.5), (5.12) and (5.13). Note that [38] only gave results for $\theta \in [0, \pi]$, and since our reduced problem is purely symmetric, we can replace θ with $|\theta|$ to get correct results for $\theta \in [-\pi, \pi]$. Their uniform approximation (given by equation (5.14)) as well as some other similar ones can be derived using

the same methodology followed by Nethercote *et al*. [50] to obtain a uniform geometric theory of diffraction approximation for a perfect wedge problem.

We take the uniform approximation from [38, eq. (5.14)] and apply Foldy's approximation, while noting that in our context $\zeta_m = \sqrt{2kr}\sin(\frac{1}{2}(|\theta| - \varphi_m))$. Therefore, we obtain

$$\Phi_S \approx -I(\theta)\sqrt{\frac{2}{\pi kr}}\,\mathrm{e}^{\mathrm{i}kr-\frac{\mathrm{i}\pi}{4}} + \frac{\mathrm{e}^{\mathrm{i}kr+(\mathrm{i}\pi/4)}}{\sqrt{2\pi kr}\sin(|\theta|/2)} - \Phi_S^{(\sim 0)} + \sum_{\varphi_n\in\mathbb{R}}\left[\frac{\mathrm{e}^{\mathrm{i}kr+(i\pi/4)}}{\sqrt{\pi kr\sin(\varphi_n)\sin(\theta-\varphi_n)}} - \Phi_S^{(\sim\varphi_n)}\right]. \tag{3.15}$$

Here, $\Phi_S^{(\sim 0)}(r,\theta)$ can be expressed in terms of the Fresnel integral $\mathcal{F}(z)$ from the scaled complex error function $w(z)$ by using [48, eqn (7.5.9)],

$$\begin{aligned}\Phi_S^{(\sim 0)} &= \mathrm{e}^{\mathrm{i}kr}w\left(\sqrt{2kr}\sin\left(\frac{|\theta|}{2}\right)\mathrm{e}^{(\mathrm{i}\pi/4)}\right)\\ &= \mathrm{e}^{\mathrm{i}kr\cos(\theta)}\left[1-(1-\mathrm{i})\mathcal{F}\left(2\sqrt{\frac{kr}{\pi}}\sin\left(\frac{|\theta|}{2}\right)\right)\right],\end{aligned} \tag{3.16}$$

where $\mathcal{F}(z)$ is given by (7.2.7) + i(7.2.8) from [48], i.e. $\mathcal{F}(z) = \int_0^z \mathrm{e}^{(\mathrm{i}\pi/2)t^2}\,\mathrm{d}t$. The other term $\Phi_S^{(\sim\varphi_n)}(r,\theta)$ is expressed in terms of the parabolic cylinder function $D_{-1/2}(z)$ of order $-\frac{1}{2}$ by the formulae,

$$\Phi_S^{(\sim\varphi_n)} = \frac{\mathrm{e}^{\mathrm{i}kr\cos^2((|\theta|-\varphi_n)/2)+(\mathrm{i}\pi/8)}}{(kr)^{1/4}\sqrt{\pi\sin(\varphi_n)\cos((|\theta|-\varphi_n)/2)}}D_{-1/2}\left(2\sqrt{kr}\sin(|\theta|-\varphi_n/2)\,\mathrm{e}^{-(\mathrm{i}\pi/4)}\right). \tag{3.17}$$

There are similar uniform approximations in [30] but with $\sin((|\theta|-\varphi_n)/2)$ replaced by $(|\theta|-\varphi_n)/2$. However, these approximations are more locally uniform as they quickly become invalid as you move away from the singularity they remove. Here, the definition of the parabolic cylinder function (see [49, eqn (9.241.1)]) is given by

$$D_{-1/2}(z) = \frac{\mathrm{e}^{(z^2/4)+(\mathrm{i}\pi/4)}}{\sqrt{2\pi}}\int_{-\infty}^{\infty}\frac{\mathrm{e}^{-(t^2/2)+\mathrm{i}zt}}{\sqrt{t}}\,\mathrm{d}t, \tag{3.18}$$

where the square root is restricted to the principal branch. It is possible to write the parabolic cylinder function in terms of Hankel functions,

$$D_{-1/2}(z\,\mathrm{e}^{-(\mathrm{i}\pi/4)}) = \mathrm{i}\sqrt{\frac{\pi z}{8}}H_{1/4}^{(1)}\left(\frac{z^2}{4}\right), \quad |\arg(z)| \le \frac{\pi}{2}, \tag{3.19}$$

by using [48, eqns. (12.7.10) and (10.27.8)]. Equation (3.19) can then be analytically continued to the left half-plane using [49, eqn (8.476.6)] with $m = 2$ and $\nu = 1/4$,

$$D_{-1/2}(z\,\mathrm{e}^{-(\mathrm{i}\pi/4)}) = \mathrm{i}\sqrt{-\frac{\pi z}{8}}\left[H_{1/4}^{(1)}\left(\frac{z^2}{4}\right) - 2(1+\mathrm{i})J_{1/4}\left(\frac{z^2}{4}\right)\right], \quad \frac{\pi}{2} < |\arg(z)| \le \frac{3\pi}{2}. \tag{3.20}$$

Note that the square roots in (3.19) and (3.20) are restricted to the principal branch and $J_n(z)$ represents the Bessel function of the first kind. We express the parabolic cylinder function in this way because it is not formally programmed for software such as MATLAB (to the authors' knowledge at least), and these connection equations provide a simple and convenient formula for us to use, which is valid for all arguments required.

Figure 6 also compares this uniform far-field approximation with the non-uniform version and the Hankel summation. Note that in our plot, the uniform approximation is continuous but not differentiable at $\theta = \pm\varphi_{-1}$ due to the branch point behaviour there. This results in a small but unwanted error around these points. This is in contrast to fig. 5.5 of [38] which appears to be differentiable. We believe that this is due to an approximation (given by equation (5.10)) that they use in their result.

In order to address this issue, we will consider higher order asymptotic approximations. We can achieve this either by using the original expansion of the integrand (3.9),

$$I^{(\sim)}(\varphi;\varphi_n)=\frac{\mathrm{e}^{(\mathrm{i}\pi/4)}}{\sqrt{-2\mathrm{i}(\cos(\varphi_n)-\cos(\varphi))}}\times\left(\frac{1}{1+((1+\mathrm{i})/2)ks\mathcal{K}_1\sqrt{-\mathrm{i}(\cos(\varphi_n)-\cos(\varphi))}-\mathrm{i}\mathcal{K}_2(\cos(\varphi_n)-\cos(\varphi))}\right), \tag{3.21}$$

or a simplified one,

$$I^{(\sim)}(\varphi;\varphi_n)=\frac{\mathrm{e}^{(\mathrm{i}\pi/4)}}{\sqrt{-2\mathrm{i}(\cos(\varphi_n)-\cos(\varphi))}}, \tag{3.22}$$

with the latter leading to (3.15). It is important to note that the expansion that gives us (3.22) requires $|((1+\mathrm{i})/2)ks\mathcal{K}_1\sqrt{-\mathrm{i}(\cos(\varphi_n)-\cos(\varphi))}-\mathrm{i}\mathcal{K}_2(\cos(\varphi_n)-\cos(\varphi))|<1$ to be valid, which breaks down if ka is too small because $\mathcal{K}_1$ (and the whole expression) is $O(\ln(ka))$ as $ka\to 0$. We then add and subtract $I^{(\sim)}$ inside the integrand of the scattered wave (3.2) for every real φ_n,

$$\begin{aligned}\Phi_S&=\frac{1}{\pi}\int_{\pi-\mathrm{i}\infty}^{\mathrm{i}\infty}\left(I(\varphi)-\sum_{\varphi_n\in\mathbb{R}}[I^{(\sim)}(\varphi;\varphi_n)]+\sum_{\varphi_n\in\mathbb{R}}[I^{(\sim)}(\varphi;\varphi_n)]\right)\mathrm{e}^{\mathrm{i}kr\cos(|\theta|-\varphi)}\mathrm{d}\varphi,\\&=\frac{1}{\pi}\int_{(\pi/2)-\mathrm{i}\infty}^{-(\pi/2)+\mathrm{i}\infty}\left(I(\varphi+|\theta|)-\sum_{\varphi_n\in\mathbb{R}}[I^{(\sim)}(\varphi+|\theta|;\varphi_n)]\right)\mathrm{e}^{\mathrm{i}kr\cos(\varphi)}\mathrm{d}\varphi\\&\quad+\sum_{\varphi_n\in\mathbb{R}}\frac{1}{\pi}\int_{(\pi/2)-\mathrm{i}\infty}^{-(\pi/2)+\mathrm{i}\infty}I^{(\sim)}(\varphi+|\theta|;\varphi_n)\,\mathrm{e}^{\mathrm{i}kr\cos(\varphi)}\,\mathrm{d}\varphi.\end{aligned} \tag{3.23}$$

To obtain (3.23), we transformed the integral with the substitution $\varphi=\varphi'+|\theta|$, deformed the contour to the local steepest descent path through the saddle point at $\varphi'=0$ (taking care to divert around intercepted branch cuts), and dropped the prime from φ'. The first integral in (3.23) is approximated using the method of steepest descent. This approximation results only in saddle point contributions since the branch cut contributions are cancelled out. This leads to the following expression:

$$\begin{aligned}\Phi_S&=-\sqrt{\frac{2}{\pi kr}}\left[I(|\theta|)-\sum_{\varphi_n\in\mathbb{R}}I^{(\sim)}(|\theta|;\varphi_n)\right]\mathrm{e}^{\mathrm{i}kr-(\mathrm{i}\pi/4)}\\&\quad+\sum_{\varphi_n\in\mathbb{R}}\frac{1}{\pi}\int_{(\pi/2)-\mathrm{i}\infty}^{-(\pi/2)+\mathrm{i}\infty}I^{(\sim)}(\varphi+|\theta|;\varphi_n)\,\mathrm{e}^{\mathrm{i}kr\cos(\varphi)}\mathrm{d}\varphi.\end{aligned} \tag{3.24}$$

Creating an approximation in this way is beneficial because the subtraction of $I^{(\sim)}$ will remove the singularities (at $|\theta|=\varphi_n$) present in the non-uniform approximation (3.14) due to I. The addition of $I^{(\sim)}$ afterwards serves as a correction to ensure equivalence with the original scattered wave. This addition must be evaluated either analytically (leading to terms similar to (3.16) and (3.17)) or through numerical integration on the steepest descent path (while taking care to navigate around branch cuts) to ensure uniformity at the removed singularities. For brevity, we will only use numerical integration here. We compare this uniform approximation with the Hankel summation, the non-uniform far-field approximations as well as the uniform approximation given by Linton *et al*. [38, eqn (5.14)] in figure 6. This plot shows that this new approximation is more accurate and smoother than the others at $|\theta|=\varphi_n$, while remaining excellent elsewhere.

Double resonance: As in the infinite array problem, double resonance occurs when both resonance conditions are satisfied at the same time, implying that ks is a multiple of π. Generally, when ks is a multiple of π, we find that the branch points of the Wiener–Hopf kernel will coalesce. In the appendix, we explain that the kernel has two branch cuts emerging from the same point (A 10) (for example, see figure 9*b*). This also changes the branch points of the kernel

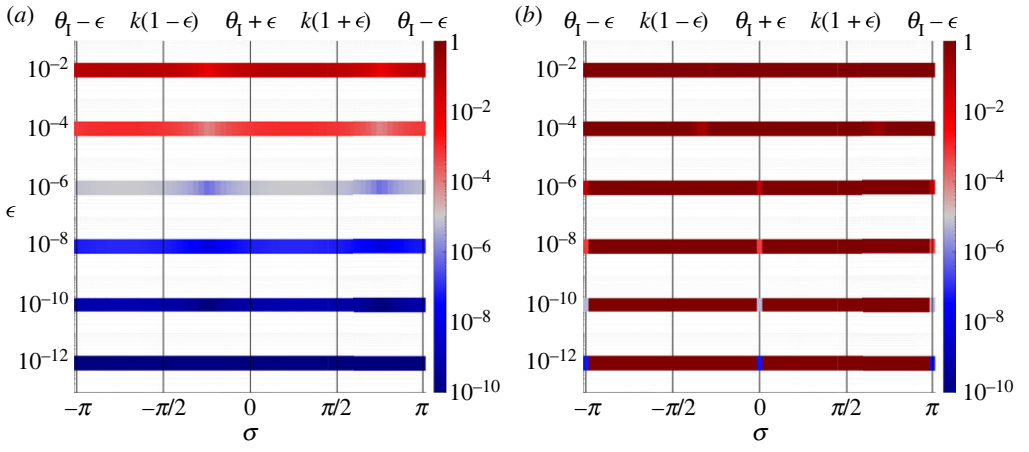

Figure 7. Visualization of the wave field uniqueness for the semi-infinite array problem at $(r, \theta) = (10\,s, \pi/4)$, where $s = 0.1$ and $a = 0.001$. (*a*) A non-resonant case, which has a unique limit, where $k = 40\pi/3$ and $\theta_I = \pi/2$. (*b*) A double resonance case, which does not have a unique limit, where $k = 40\pi$ and $\theta_I = 2\pi/3$. (Online version in colour.)

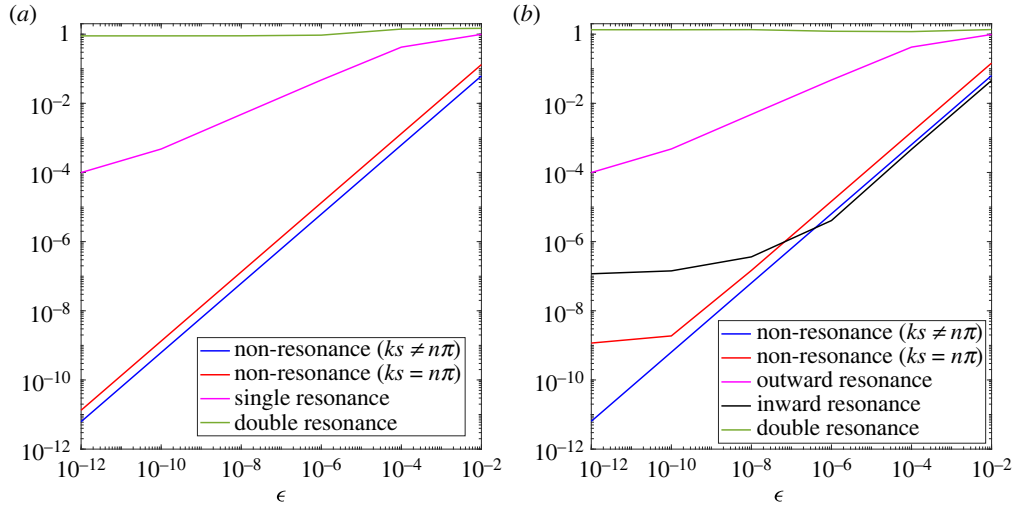

Figure 8. Plots of the averages of each of the colour bars displayed in figure 2 and figure 7 as $\epsilon \to 0^+$. (*a*) Non-resonant cases as well as single and double resonance cases for the infinite array problem. (*b*) Non-resonant cases as well as outward, inward and double resonance cases for the semi-infinite array problem. (Online version in colour.)

factors from square-root to fourth-root (see (A 11)), which is a drastic change in behaviour. For non-resonant cases, this has a cascading effect on the long-term behaviour of the scattering coefficients and the tail-end of the Hankel summation (3.1). We also expect similar effects for double resonance. As far as the authors are aware, there are not many articles that look into double resonance in this context. Neither [14] nor [30] considered double resonance but [29] obtained some interesting results by looking at the far-field asymptotics of the scattered field as the incident angle approaches one that induces double resonance. Their final result implies that $\Phi_S \sim -e^{-ikr\cos(\theta)}$ for $kr \gg 1$ and the author conjectured that the results are valid for all kr, meaning that in the double resonance limit, the total field is equivalent to the outward resonance case (3.5). In other words, the outward and inward resonant waves are not superimposed in contrast to the infinite array problem. Millar also acknowledged that they did not consider what happens if ks

approaches a value to induce double resonance. However, the drastic behaviour change resulting from the branch points coalescing allows for the reasonable assertion that a perturbed ks will not tend to the same solution as a perturbed θ_I which implies that this case does not have a unique solution. This is what we propose to illustrate in the next subsection.

(a) Discussions on uniqueness/non-uniqueness

In this section, we visualize uniqueness or non-uniqueness for the semi-infinite array problem, for which we use the same methodology as in the infinite array problem (see §2a). For the non-resonance and outward resonance cases, we use (3.4) to assess uniqueness but with one small change. In the pole summation, we also include the first complex values of $\varphi_n^{(\mathrm{pole})}$ as well as all the real ones ($\varphi_n^{(\mathrm{pole})} \in \mathbb{R}$). This is particularly important during outward resonance as one $\varphi_n^{(\mathrm{pole})}$ is on the borderline of being purely real and becomes the dominant term in the equation. Under the original condition, some perturbations will still include the borderline value of $\varphi_n^{(\mathrm{pole})}$ but there are others which will give it a small imaginary part, therefore not satisfying the condition. This is why we edited (3.4) to include the first complex values of $\varphi_n^{(\mathrm{pole})}$, to keep as much continuity as possible for all perturbation directions. For the inward and double resonance cases, we would not be able to use (3.4) because the branch point and pole singularities are combined which renders this invalid. Hence, we shall revert to the Hankel summation for these cases.

Figure 7 visualizes the solution uniqueness for the semi-infinite array problem. Similarly to figure 2, it includes a non-resonant case where $ks \neq n\pi$ (*a*) and a double resonance case (*b*). Figure 8*b* shows the average of the bars for several different cases (*b*). This plot also includes two non-resonant cases as well as an example of outward, inward and double resonance cases. We find that both the non-resonant cases as well as the outward and inward resonance cases are converging, implying uniqueness. Although it is important to note that, outward and inward resonance converge more slowly than non-resonant cases and are more susceptible to numerical error. As in the infinite array problem, we see that the double resonance case is not converging to a unique solution. Unlike the infinite array problem, the perturbation of θ_I does not lead to non-uniqueness. In other words, both of the perturbations $\theta_\mathrm{I} + \epsilon$ and $\theta_\mathrm{I} - \epsilon$ lead to the same solution which is not the case for the infinite array problem. This conjecture is backed up by figure 7*b* and the conclusions of [29].

4. Conclusion

In this article, we have provided a brief overview of the special resonance cases for wave scattering by infinite and semi-infinite arrays in the context of Foldy's approximation. From this overview, we recovered several known results for different resonance cases (including single and double resonance in both problems), and derived a new asymptotic approximation for inward resonance in the semi-infinite array problem.

For the infinite array problem, we verified the well-known single resonance solution from the scattering angle formula (2.4) and validated the non-uniqueness of the double resonance solution in the context of Foldy's approximation. We then showed how the amplitudes of the resonant waves are dependent on the direction in which the double resonance limit is approached, and in doing so, it became possible to recover solutions that have appeared in the previous literature. However, it is clear that the non-uniqueness is due to a breakdown of Foldy's approximation, and the different values for the resonant amplitudes do not appear to have any physical meaning. Including dipole terms (and possibly higher order terms) leads to a unique solution in all cases as shown by Linton & Thompson [28] and appendix C. We also developed a way to visualize this non-uniqueness (figure 2), which further demonstrated our conclusions.

For the semi-infinite array problem, we recovered the known solution in the outward resonance case and a non-uniform far-field approximation for the inward resonance case. When simplified by Foldy's approximation (to compare it with our results), the uniform

far-field approximation discovered by Linton *et al*. [38] turns out not to be continuously differentiable across the shadow boundaries $|\theta| = \varphi_n \neq 0$. This was missable in their article due to an approximation used for their numerical results. To alleviate the shortcomings of this approximation, we considered higher-order terms and improved the overall accuracy and smoothness of the uniform far-field approximation (figure 6). For the double resonance case, we determined that the solution is only unique if ks remains fixed. This was verified using the same visualizations as in the infinite array problem (figure 7). We surmised that this non-uniqueness is also likely due to using Foldy's approximation.

The results and assessments of this article will be important for future research. Specifically, we plan to piece these results together with our work on the point scatterer wedge [17] to study potential resonance cases. In that article, we asserted that there could be at least four resonance conditions given by (4.1), two for the top array and two for the bottom array, respectively. The results of this article show us the resonance effects of isolated arrays, which is a step towards the overall resonance effects of point scatterer wedges and has potential applications in metamaterial and metasurface design.

Data accessibility. This article has no additional data.

Authors' contributions. M.A.N.: conceptualization, formal analysis, investigation, methodology, validation, visualization, writing—original draft, writing—review and editing; I.T.: formal analysis, investigation, methodology, validation, writing—review and editing; A.V.K.: conceptualization, formal analysis, investigation, methodology, supervision, validation, writing—review and editing; R.C.A.: conceptualization, formal analysis, investigation, methodology, supervision, validation, writing—review and editing.

All authors gave final approval for publication and agreed to be held accountable for the work performed therein.

Conflict of interest declaration. We declare we have no competing interests.

Funding. A.V.K. is supported by a Royal Society Dorothy Hodgkin Research Fellowship and a Dame Kathleen Ollerenshaw Fellowship, through which M.A.N. has been funded. M.A.N., A.V.K. and R.C.A. are also funded by EPSRC grant no. EP/W018381/1.

Appendix A. Branch point asymptotics for the discrete Wiener–Hopf kernel and its factors

We already know from [17] that the discrete Wiener–Hopf kernel

$$K(z) = H_0^{(1)}(ka) + \sum_{\ell=1}^{\infty}(z^{\ell} + z^{-\ell})H_0^{(1)}(ks\ell) \tag{A 1}$$

has two branch point singularities at $z = \mathrm{e}^{\pm \mathrm{i}ks}$, however, it will be useful to get a sense of their nature and the effect on the factorization of their asymptotic behaviour. Unfortunately, when k is real, (A 1) is only convergent on the unit circle except for the branch points. As a result, it is not the best formula to use in order to determine the asymptotic behaviour we are looking for. Instead, we will substitute $z = \mathrm{e}^{\mathrm{i}t}$ and use an alternative and more rapidly convergent formula in the t complex plane (see [17, eqn. (A 7)]) given by

$$\begin{aligned} K(\mathrm{e}^{\mathrm{i}t}) = H_0^{(1)}(ka) - 1 - \frac{2\mathrm{i}}{\pi}\left(\gamma + \ln\left(\frac{ks}{4\pi}\right)\right) + \frac{2}{\mathrm{i}\sqrt{-\mathrm{i}(ks-t)}\sqrt{-\mathrm{i}(ks+t)}} \\ + \sum_{\substack{\ell=-\infty \\ \ell\neq 0}}^{\infty}\left(\frac{2}{\mathrm{i}\sqrt{-\mathrm{i}(ks-(2\pi\ell - t))}\sqrt{-\mathrm{i}(ks+(2\pi\ell - t))}} + \frac{\mathrm{i}}{\pi|\ell|}\right), \end{aligned} \tag{A 2}$$

where $\gamma = 0.5772\cdots$ is the Euler–Mascheroni constant and all square roots are defined using the principal branch. The formula (A 2) is convergent for complex t and is an analytic continuation of (A 1) from the z unit circle to the entire complex plane (except the branch points and cuts). Here, the branch points are periodically located at $t = \pm ks + 2\pi\ell$ ($\ell \in \mathbb{Z}$) with respective branch cuts directed towards $\pm ks + 2\pi\ell \pm \mathrm{i}\infty$ (due to the $-\mathrm{i}$ factor). In other words, the branch is chosen such

that if $t \mp ks - 2\pi\ell > 0$, then $\arg\left(\sqrt{-\mathrm{i}(ks \pm (2\pi\ell - t))}\right) = \pm(\mathrm{i}\pi/4)$. As $t \to \pm ks$, only one square root term becomes dominant. Hence, $K(\mathrm{e}^{\mathrm{i}t})$ has the following asymptotic behaviour:

$$K(\mathrm{e}^{\mathrm{i}t}) = \sqrt{\frac{2}{ks}}\frac{\mathrm{e}^{-(\mathrm{i}\pi/4)}}{\sqrt{-\mathrm{i}(ks \mp t)}} + \mathcal{K}_1 + \frac{\mathrm{e}^{(\mathrm{i}\pi/4)}\sqrt{-\mathrm{i}(ks \mp t)}}{(2ks)^{3/2}} + O(ks \mp t), \tag{A 3}$$

where

$$\begin{aligned}\mathcal{K}_1 = H_0^{(1)}(ka) - 1 - \frac{2\mathrm{i}}{\pi}\left(\gamma + \ln\left(\frac{ks}{4\pi}\right)\right) \\ + \sum_{\ell=1}^{\infty}\left(\frac{1}{\sqrt{\pi\ell(ks - \pi\ell)}} + \frac{1}{\mathrm{i}\sqrt{\pi\ell(ks + \pi\ell)}} + \frac{2\mathrm{i}}{\pi\ell}\right).\end{aligned} \tag{A 4}$$

Note that all square roots in (A 3) and (A 4) take the principal branch. When written in the t plane, the kernel factors are given by the identity $K^-(\mathrm{e}^{\mathrm{i}t}) = K^+(\mathrm{e}^{-\mathrm{i}t})$, and the formula

$$\begin{aligned}\ln(K^+(\mathrm{e}^{\mathrm{i}t})) = \ln(K_0) - \frac{1}{2\pi}\int_{-\pi}^{\pi}\frac{\ln(K(\mathrm{e}^{\mathrm{i}\tau}))}{1 - \mathrm{e}^{-\mathrm{i}(\tau + t)}}\,\mathrm{d}\tau, \\ \text{where} \quad \ln(K_0) = \frac{1}{2\pi}\int_0^{\pi}\ln(K(\mathrm{e}^{\mathrm{i}\tau}))\,\mathrm{d}\tau.\end{aligned} \tag{A 5}$$

Here, the integration contour follows a path illustrated on figure 9*a*. Note that we cannot rule out the possibility that $K(\mathrm{e}^{\mathrm{i}t}) = 0$ for some complex t. It has been proven that a zero when t is real indicates the presence of a Rayleigh–Bloch wave which cannot happen with Dirichlet boundary conditions (see [40] for a rigorous proof). Because there are no isolated zeros on the real line, we can say that there exists a neighbourhood of the real line in which we can safely deform the contour to the path on figure 9*a* without encountering zeros. When the Wiener–Hopf kernel is factorized, each factor takes the asymptotic behaviour of one branch point and is analytic on the other. For example, the K^+ factor keeps the branch point at $t = -ks$ but is analytic on $t = ks$ (and vice versa for the K^- factor). Noting that $K^+(\mathrm{e}^{\mathrm{i}t}) = (K(\mathrm{e}^{\mathrm{i}t})/K^+(\mathrm{e}^{-\mathrm{i}t}))$, we find that the asymptotic behaviour for the K^+ factor as $t \to -ks$ is given by

$$\begin{aligned}K^+(\mathrm{e}^{\mathrm{i}t}) &= \frac{1}{K^+(\mathrm{e}^{\mathrm{i}ks})}\left(1 + \mathrm{i}\,\mathrm{e}^{\mathrm{i}ks}\frac{K^{+'}(\mathrm{e}^{\mathrm{i}ks})}{K^+(\mathrm{e}^{\mathrm{i}ks})}(ks + t) + O((ks + t)^2)\right) \times (\mathrm{A}\,3), \\ &= \frac{1}{K^+(\mathrm{e}^{\mathrm{i}ks})}\left[\sqrt{\frac{2}{ks}}\frac{\mathrm{e}^{-(\mathrm{i}\pi/4)}}{\sqrt{-\mathrm{i}(ks + t)}} + \mathcal{K}_1 + \frac{\mathrm{e}^{(\mathrm{i}\pi/4)}\sqrt{-\mathrm{i}(ks + t)}}{(2ks)^{3/2}}\right. \\ &\quad \left.\times\left(1 + 4\,\mathrm{i}ks\,\mathrm{e}^{\mathrm{i}ks}\frac{K^{+'}(\mathrm{e}^{\mathrm{i}ks})}{K^+(\mathrm{e}^{\mathrm{i}ks})}\right) + O(ks + t)\right],\end{aligned} \tag{A 6}$$

where the ratio $K^{+'}(\mathrm{e}^{\mathrm{i}ks})/K^+(\mathrm{e}^{\mathrm{i}ks})$ is obtained by differentiating (A 5) with respect to t and also uses the same contour path,

$$\frac{K^{+'}(\mathrm{e}^{\mathrm{i}ks})}{K^+(\mathrm{e}^{\mathrm{i}ks})} = \frac{1}{2\pi}\int_{-\pi}^{\pi}\frac{\ln(K(\mathrm{e}^{\mathrm{i}\tau}))}{(\mathrm{e}^{\mathrm{i}(ks + \tau)} - 1)^2}\,\mathrm{e}^{\mathrm{i}\tau}\,\mathrm{d}\tau. \tag{A 7}$$

A similar formula for the K^- factor as $t \to ks$ can be obtained using the identity $K^+(\mathrm{e}^{\mathrm{i}t}) = K^-(\mathrm{e}^{-\mathrm{i}t})$, but we do not do it here. The behaviour (A 3) breaks down when ks is an integer multiple of π. In this situation, two of the branch points in the t plane have coalesced which means that two branch cuts emerge from the same branch point (figure 9*b*). This implies that two square root

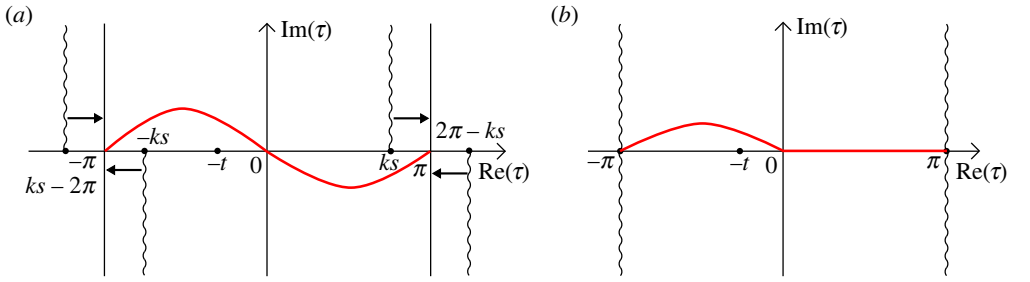

Figure 9. Diagrams of the integration contours (in red) used in (A 5) (*a*) and an example illustrating the branch points coalescing as $ks \to \pi$ (*b*).

terms equally dominate the asymptotic behaviour of the $K(e^{it})$ as $t \to \pm ks$ even though they have different branch definitions. That behaviour is given by

$$\begin{aligned} K(e^{it}) &= \frac{2}{\sqrt{(ks)^2 - t^2}} + \frac{2}{\sqrt{(ks)^2 - (2ks - t)^2}} + \mathcal{K}_\pi + O(\sqrt{ks \mp t}), \\ &= \sqrt{\frac{2}{ks}} \frac{e^{-(i\pi/4)}}{\sqrt{-i(ks \mp t)}} + \sqrt{\frac{2}{ks}} \frac{e^{-(i\pi/4)}}{\sqrt{i(ks \mp t)}} + \mathcal{K}_\pi + O(\sqrt{ks \mp t}), \end{aligned} \tag{A 8}$$

where

$$\begin{aligned} \mathcal{K}_\pi = H_0^{(1)}(ka) - 1 - \frac{2i}{\pi}\left(\gamma + \ln\left(\frac{ks}{4\pi}\right)\right) + \frac{1}{iks\sqrt{2}} + \frac{2i}{ks} \\ + \sum_{\substack{\ell=1 \\ \ell \neq \frac{ks}{\pi}}}^{\infty} \left(\frac{1}{\sqrt{\pi\ell(ks - \pi\ell)}} + \frac{1}{i\sqrt{\pi\ell(ks + \pi\ell)}} + \frac{2i}{\pi\ell} \right). \end{aligned} \tag{A 9}$$

Alternatively, if we were to use the relation

$$\sqrt{-iz} + \sqrt{iz} = \left((\sqrt{-iz} + \sqrt{iz})^4 \right)^{1/4} = (4z^2)^{1/4} = \sqrt{2}(iz)^{1/4}(-iz)^{1/4},$$

we can write (A 8) in a way that is much more suitable for factorization,

$$K(e^{it}) = \frac{2}{\sqrt{ks}} \left(\frac{1}{-i(ks \mp t)} \right)^{1/4} \left(\frac{1}{i(ks \mp t)} \right)^{1/4} e^{-(i\pi/4)} + \mathcal{K}_\pi + O(\sqrt{ks \mp t}). \tag{A 10}$$

Note that the fourth roots all take the principal branch as well. When we factorize (A 10) about $t = -ks$, we assign $(-i(ks + t))^{-1/4}$ to the $K^+(e^{it})$ factor, then $(i(ks + t))^{-1/4}$ will be assigned to $K^-(e^{2iks + it}) = K^-(e^{it})$ (because $i(ks + t) = -i(ks - (2ks + t))$). This means that if ks is a multiple of π then the asymptotic behaviour of the $K^+(z)$ factor as $t \to -ks$ is given by,

$$\begin{aligned} K^+(e^{it}) = \left(\frac{4i}{ks(ks + t)} \right)^{1/4} e^{-(i\pi/8)} \\ + \mathcal{K}_\pi \frac{(ks)^{1/4}}{2} e^{(i\pi/8)}(-i(ks + t))^{1/4} + O((ks + t)^{3/4}), \end{aligned} \tag{A 11}$$

where a similar formula is obtained for the K^- factor as $t \to ks$ using $K^+(e^{it}) = K^-(e^{-it})$.

Appendix B. Linking the semi-infinite array to Sommerfeld's half-plane

In this appendix, we want to link the semi-infinite array problem to Sommerfeld's half-plane problem by matching the integral solution given by (3.2) to the equivalent for the half-plane given by

$$\Phi_S(r,\theta) = \frac{1}{\pi\,\mathrm{i}} \int_{\pi-\mathrm{i}\infty}^{\mathrm{i}\infty} \frac{\sin(\theta_\mathrm{I}/2)\sin(\varphi/2)}{\cos(\varphi)+\cos(\theta_\mathrm{I})}\, \mathrm{e}^{\mathrm{i}kr\cos(|\theta|-\varphi)}\,\mathrm{d}\varphi. \tag{B 1}$$

This solution is found using the continuous Wiener–Hopf technique detailed in [51] (although it should be noted that a geometry transform is required as this book has the half-plane on the negative x-axis instead). For now, we shall restrict $\theta_\mathrm{I} \in [0,\pi]$ for brevity. The integration contour of (B 1) has the same definition as (3.2) and is indented above the simple pole at $\varphi = \pi - \theta_\mathrm{I}$.

To match the semi-infinite array to the half-plane, we must take the limit $s \to 0$ while keeping $a \ll s/2$ in place and show that the limiting form of the integrand in (3.2) is equal to (B 1). To do this, we need to know the asymptotic behaviour of $K^+(\mathrm{e}^{\mathrm{i}ks\tau})$ for small s. Take (A 2) with $t = ks\tau$ and $a \ll s/2 \ll 1$, then

$$K(\mathrm{e}^{\mathrm{i}ks\tau}) = \frac{2}{\mathrm{i}ks\sqrt{-\mathrm{i}(1-\tau)}\sqrt{-\mathrm{i}(1+\tau)}} + \frac{2\mathrm{i}}{\pi}\ln\left(\frac{2\pi a}{s}\right) + O(ks). \tag{B 2}$$

If $\lim_{s\to 0} |ks\ln(\frac{a}{s})| = \infty$, then the logarithmic term dominates (B 2). In this case, the scatterer sizes are decreasing too quickly for a half-plane to form and as a result, the scattered field tends to zero. If $\lim_{s\to 0} |ks\ln(a/s)| = 0$, then the square root term dominates

$$K(\mathrm{e}^{\mathrm{i}ks\tau}) \sim \frac{2}{\mathrm{i}ks\sqrt{-\mathrm{i}(1-\tau)}\sqrt{-\mathrm{i}(1+\tau)}}. \tag{B 3}$$

This can be factorized fairly simply. The K^+ factor should have a branch point at $\tau = -1$ and be analytic at $\tau = 1$, hence,

$$K^+(\mathrm{e}^{\mathrm{i}ks\tau}) \sim \sqrt{\frac{2}{\mathrm{i}ks}}\,\frac{1}{\sqrt{-\mathrm{i}(1+\tau)}}. \tag{B 4}$$

We apply (B 4) to the integrand of (3.2) and then as $s \to 0$

$$\begin{aligned}\frac{1}{K^+(\mathrm{e}^{-\mathrm{i}ks\cos(\theta_\mathrm{I})})K^+(\mathrm{e}^{-\mathrm{i}ks\cos(\varphi)})(1-\mathrm{e}^{-\mathrm{i}ks(\cos(\varphi)+\cos(\theta_\mathrm{I}))})} &\sim \frac{\sqrt{-\mathrm{i}(1-\cos(\theta_\mathrm{I}))}\sqrt{-\mathrm{i}(1-\cos(\varphi))}}{2(\cos(\varphi)+\cos(\theta_\mathrm{I}))},\\ &\sim \frac{\sin(\theta_\mathrm{I}/2)\sin(\varphi/2)}{\mathrm{i}(\cos(\varphi)+\cos(\theta_\mathrm{I}))},\end{aligned} \tag{B 5}$$

which completes the link between the semi-infinite array and Sommerfeld's half-plane. If $\lim_{s\to 0} |ks\ln(a/s)| = c > 0$, which could happen if $a(s) = s\,\mathrm{e}^{-(c/ks)}$ for instance, then factorizing (B 2) is not a simple task [52]. However, it can be argued that this is a transition region between the semi-infinite array turning into a half-plane and disappearing entirely. This is evident in (3.4) where the amplitude of the only propagating wave simplifies to,

$$\lim_{s\to 0}\left(-\frac{2}{ksK(\mathrm{e}^{-\mathrm{i}ks\cos(\theta_\mathrm{I})})\sin(\varphi_0^{(\mathrm{pole})})}\right) = -\frac{1}{1-(\mathrm{i}c/\pi)\sin(\theta_\mathrm{I})}. \tag{B 6}$$

Here, $c = 0$ recovers the amplitude for the geometrical optic component of the half-plane problem and $c \to \infty$ leads to the plane wave (with the entire scattered field) tending to zero, symbolizing the semi-infinite array's disappearance. It is worth noting that all of these conclusions apply to the infinite array matching to an infinite plane as well.

Appendix C. Full linear theory

Diffraction by linear arrays of circular cylinders at resonant frequencies was considered by Linton & Thompson [28], without the restriction $ka \ll 1$. There the calculation was performed by considering unknown quantities such as grating mode amplitudes as functions of the scattering angles. Here, we show how a slight modification of the method allows the same results to be obtained without the need to take limits, or to vary any parameter in particular, as resonance (single or double) is approached. We then derive an explicit solution that is valid at low frequency and show that this leads to (2.10). The argument presented here does *not* amount to a full proof

of uniqueness for the array problem. In particular, it does not rule out the existence of Rayleigh–Bloch waves or other types of trapped mode. Our intention is to show that the non-uniqueness observed in §2 is due to a breakdown of the point scatterer model. The fact that no trapped modes can exist on a linear array of cylinders subject to Dirichlet boundary conditions was established in [40].

Following [28], we represent the field in the form

$$\Phi = \mathrm{e}^{-\mathrm{i}kr\cos(\theta-\theta_1)} + \sum_{j=-\infty}^{\infty} \mathrm{e}^{-\mathrm{i}jks\cos(\theta_1)} \sum_{n=-\infty}^{\infty} B_n H_n^{(1)}(kr_j)\,\mathrm{e}^{\mathrm{i}n\theta_j}, \tag{C 1}$$

where (r_j, θ_j) is a set of polar coordinates with its origin at the centre of cylinder j, so that

$$r_j\cos(\theta_j) = x - js, \quad r_j\sin(\theta_j) = y \quad \text{and} \quad (r_0, \theta_0) = (r, \theta).$$

Note that we have defined the incident wave as in §2, which is different to [28]. The incident and scattered fields are then expanded about the central scatterer using the Jacobi–Anger expansion [53, eqn 2.17], and Graf's addition theorem [53, theorem 2.12], respectively. This leads to

$$\begin{aligned}\Phi = &\sum_{m=-\infty}^{\infty} ((-i)^m J_m(kr)\,\mathrm{e}^{\mathrm{i}m(\theta-\theta_1)} + B_m H_m^{(1)}(kr)\,\mathrm{e}^{\mathrm{i}m\theta}) \\ &+ \sum_{\substack{j=-\infty \\ j\neq 0}}^{\infty} \left(\mathrm{e}^{-\mathrm{i}jks\cos(\theta_1)} \sum_{n=-\infty}^{\infty} B_n \sum_{m=-\infty}^{\infty} H_{n-m}^{(1)}(|j|ks)(-\mathrm{sgn}(j))^{n-m} J_m(kr)\,\mathrm{e}^{\mathrm{i}m\theta} \right), r < s,\end{aligned} \tag{C 2}$$

where the term with $j = 0$ is left unchanged, because it is already in the correct form in (C 1). Finally, orthogonality in θ is applied, and the Dirichlet boundary condition enforced on $r = a$, leading to the linear system of equations

$$B_m + Z_m \sum_{n=-\infty}^{\infty} B_n \sigma_{n-m} = -Z_m(-\mathrm{i})^m\,\mathrm{e}^{-\mathrm{i}m\theta_1}, \quad m \in \mathbb{Z}. \tag{C 3}$$

Here, the Z_m coefficients are given by $Z_m = J_m(ka)/H_m^{(1)}(ka)$, and the Schlömilch series σ_n is given by

$$\sigma_n = \sum_{j=1}^{\infty} H_n^{(1)}(jks)(\mathrm{e}^{\mathrm{i}jks\cos(\theta_1)} + (-1)^n\,\mathrm{e}^{-\mathrm{i}jks\cos(\theta_1)}). \tag{C 4}$$

Some care is needed with the notation used for Schlömilch series, because the definition of σ_n in [28] differs by a factor $(-1)^n$ from the definition used by the same authors in some later papers. Here, we use the newer definition as in [54]. Different boundary conditions can be accounted for by simply changing the coefficients Z_m (e.g. for Neumann; $Z_m = J_m'(ka)/H_m^{(1)'}(ka)$).

The field can be transformed into a sum of grating modes using an integral representation for the wave functions $H_n^{(1)}(kr_j)\,\mathrm{e}^{\mathrm{i}n\theta_j}$, (see [28, eqn (16)]). If $n = 0$ this representation is valid everywhere except the point $(x, y) = (0, 0)$; otherwise, it is valid provided that $y \neq 0$. Substituting this integral representation into (C 1) and applying the Poisson summation formula [55, p. 580] yields

$$\Phi = \mathrm{e}^{-\mathrm{i}kr\cos(\theta-\theta_1)} + \sum_{j=-\infty}^{\infty} \mathcal{A}_j^{\pm}\,\mathrm{e}^{-\mathrm{i}kr\cos(\theta\pm\psi_j)}, \quad \theta \in (-\pi, \pi], \tag{C 5}$$

where the scattering angles are defined in (2.5) and the grating mode amplitudes are given by

$$\mathcal{A}_j^{\pm} = \frac{2}{ks} \sum_{n=-\infty}^{\infty} \mathrm{i}^n B_n \frac{\mathrm{e}^{\mp\mathrm{i}n\psi_j}}{\sin(\psi_j)}. \tag{C 6}$$

Here, the upper and lower signs are to be used for $\theta > 0$ and $\theta < 0$, respectively.

If the parameters are not close to a resonance, the coefficients B_n can be computed by simply truncating (C 3), because $|Z_n| \to 0$ at an exponential rate as $|n| \to \infty$ (see (10.19.1) + i(10.19.2) from

[48]). To obtain solutions at (and near) resonance, we will separate the singular terms from the Schlömilch series σ_n, exactly as in [28]. Thus, from [54, eqns (3.37) and (3.39)], we have

$$\sigma_n = \frac{2\mathrm{i}^n}{ks}\left(\frac{\mathrm{e}^{\mathrm{i}n\psi_0}}{\sin(\psi_0)} + \sum_{\substack{j=-\infty \\ j\neq 0}}^{\infty}\left(\frac{\mathrm{e}^{\mathrm{i}n\,\mathrm{sgn}(j)\psi_j}}{\sin(\psi_j)} + \frac{\mathrm{i}\delta_{n0}}{2\pi|j|}\right)\right) + \mu_n, \quad n \geq 0, \tag{C 7}$$

where μ_n is a polynomial and δ_{n0} is the Kronecker delta. Suppose we are concerned with a potential resonance in grating mode N. Then we may define a regularized series via

$$\hat{\sigma}_n = \sigma_n - \frac{2\mathrm{i}^n\,\mathrm{e}^{\mathrm{i}n\,\mathrm{sgn}(N)\psi_N}}{ks\sin(\psi_N)}, \tag{C 8}$$

taking $\mathrm{sgn}(0) = 1$. Clearly, $\hat{\sigma}_n$ has no singularity at $\sin(\psi_N) = 0$ if $n \geq 0$. For negative indices, the Schlömilch series can be obtained via the identity $\sigma_n = (-1)^n\sigma_{-n}$, which follows directly from (C 4). Therefore, if $n < 0$, we have

$$\hat{\sigma}_n = \frac{2\mathrm{i}^n}{ks}\left(\frac{\mathrm{e}^{-\mathrm{i}n\psi_0}}{\sin(\psi_0)} + \sum_{\substack{j=-\infty \\ j\neq 0}}^{\infty}\left(\frac{\mathrm{e}^{-\mathrm{i}n\,\mathrm{sgn}(j)\psi_j}}{\sin(\psi_j)} + \frac{\mathrm{i}\delta_{n0}}{2\pi|j|}\right)\right)$$
$$+ (-1)^n\mu_{-n} - \frac{2\mathrm{i}^n\,\mathrm{e}^{\mathrm{i}n\,\mathrm{sgn}(N)\psi_N}}{ks\sin(\psi_N)}. \tag{C 9}$$

The total coefficient multiplying $\csc(\psi_N)$ is then $-4\mathrm{i}^{n+1}\mathrm{sgn}(N)\sin(n\psi_N)/(ks)$, so that the singularity is removed in all cases.

Suppose now that the parameters k, s and θ_I are such that the field is close to double resonance. Let $N_+ = (ks/2\pi)[1 - \cos(\theta_\mathrm{I})] \geq 0$ and $N_- = (ks/2\pi)[-1 - \cos(\theta_\mathrm{I})] \leq 0$ be the indices of the near-resonant modes, so that

$$|\sin\psi_j| \geq |\sin\psi_{N_\pm}|, \quad \forall j \neq N_\mp.$$

Define the regularized series

$$\hat{\sigma}_n = \sigma_n - \frac{2i^n}{ks}\left(\frac{\mathrm{e}^{\mathrm{i}n\psi_{N_+}}}{\sin(\psi_{N_+})} + \frac{\mathrm{e}^{-\mathrm{i}n\psi_{N_-}}}{\sin(\psi_{N_-})}\right), \tag{C 10}$$

which remains bounded at the double resonance. The relationship between $\hat{\sigma}_n$ and $\hat{\sigma}_{-n}$ is then

$$\hat{\sigma}_n - (-1)^n\hat{\sigma}_{-n} = \frac{4\mathrm{i}^{n+1}}{ks}\left(\frac{\sin(n\psi_{N_-})}{\sin(\psi_{N_-})} - \frac{\sin(n\psi_{N_+})}{\sin(\psi_{N_+})}\right) \tag{C 11}$$

which will be useful later. Substituting (C 10) into (C 3) yields

$$\mathrm{i}^m B_m + Z_m\sum_{n=-\infty}^{\infty} B_n\left[\mathrm{i}^m\hat{\sigma}_{n-m} + \frac{2\mathrm{i}^n}{ks}\left(\frac{\mathrm{e}^{\mathrm{i}(n-m)\psi_{N_+}}}{\sin(\psi_{N_+})} + \frac{\mathrm{e}^{-\mathrm{i}(n-m)\psi_{N_-}}}{\sin(\psi_{N_-})}\right)\right]$$
$$= -Z_m\,\mathrm{e}^{-\mathrm{i}m\theta_\mathrm{I}}, \quad m \in \mathbb{Z}. \tag{C 12}$$

Crucially, there is no need to introduce new unknowns (as was done in [28]), because the sums of the second and third terms in the square bracket are recognizable as grating mode amplitudes from (C 6). Therefore, (C 12) simplifies to

$$\mathrm{i}^m B_m + Z_m\left(\mathrm{e}^{-\mathrm{i}m\psi_{N_+}}\mathcal{A}^-_{N_+} + \mathrm{e}^{\mathrm{i}m\psi_{N_-}}\mathcal{A}^+_{N_-} + \mathrm{i}^m\sum_{n=-\infty}^{\infty} B_n\hat{\sigma}_{n-m}\right)$$
$$= -Z_m\,\mathrm{e}^{-\mathrm{i}m\theta_\mathrm{I}}, \quad m \in \mathbb{Z}. \tag{C 13}$$

In general, fixing a non-negative integer M and discarding coefficients B_n with $|n| > M$ and equations with $|m| > M$ leaves two excess unknowns in (C 13) but, from (C 6), we have

$$ks\sin(\psi_{N_\pm})\mathcal{A}^{\mp}_{N_\pm} = 2\sum_{n=-\infty}^{\infty} \mathrm{i}^n B_n \,\mathrm{e}^{\pm in\psi_{N_\pm}} \tag{C 14}$$

which closes the system.

Explicit solutions for B_n can be constructed for small values of the truncation parameter M. This is made easier if the field is separated into components that are symmetric and antisymmetric about the axis of the array (see [56]). Here, we consider only the solution at double resonance, in which case the symmetry decomposition is not needed (at least for $M \leq 1$), and we have $\psi_{N_+} = 0$ and $\psi_{N_-} = \pi$. With these values (C 11) is simplified to

$$\hat{\sigma}_n - (-1)^n\hat{\sigma}_{-n} = \frac{4n\mathrm{i}^{n-1}}{ks}(1 + (-1)^n). \tag{C 15}$$

Double resonance causes no special difficulty in (C 13), and (C 14) simplifies to

$$\sum_{n=-\infty}^{\infty} (\pm\mathrm{i})^n B_n = 0. \tag{C 16}$$

It is important to note that Foldy's approximation is equivalent to having the truncation parameter M set to zero in the full linear theory. It is immediately apparent that this fails at double resonance, because both forms of (C 16) reduce to simply $B_0 = 0$. The equation with $m = 0$ in (C 13) becomes

$$\mathcal{A}^{-}_{N_+} + \mathcal{A}^{+}_{N_-} = -1. \tag{C 17}$$

Note that there is no difference between the amplitudes on opposite sides of the grating because the scattered field is purely symmetric in this case. However, there is no further information in the model, so the solution is non-unique.

If we set $M = 1$ so that both monopoles ($n = 0$) and dipoles ($n = \pm 1$) are retained in (C 1) then, at double resonance, (C 16) yields $B_0 = 0$ as before but now also $B_{-1} = B_1$. Since (C15) shows that $\hat{\sigma}_{-1} = -\hat{\sigma}_1$ (for all parameter values), the equation in (C 13) with $m = 0$ again reduces to (C 17), but in this case, we must also include the equations with $m = \pm 1$. Using (C 15) with $n = 2$, we see that $\hat{\sigma}_{-2} = \hat{\sigma}_2 - 16\mathrm{i}/(ks)$ and so at double resonance, we have the $m = -1$ equation

$$\mathcal{A}^{-}_{N_+} - \mathcal{A}^{+}_{N_-} - \mathrm{i}B_1(Z_1^{-1} + \hat{\sigma}_0 + \hat{\sigma}_2) = -\mathrm{e}^{\mathrm{i}\theta_\mathrm{I}} \tag{C 18}$$

and

$$\mathcal{A}^{-}_{N_+} - \mathcal{A}^{+}_{N_-} + \mathrm{i}B_1\left(Z_1^{-1} + \hat{\sigma}_0 + \hat{\sigma}_2 - \frac{16\mathrm{i}}{ks}\right) = -\mathrm{e}^{-\mathrm{i}\theta_\mathrm{I}}. \tag{C 19}$$

Adding these together and using (C 17), we find that

$$\mathcal{A}^{-}_{N_+} = -\cos^2\left(\frac{\theta_\mathrm{I}}{2}\right) - \frac{4B_1}{ks} \quad \text{and} \quad \mathcal{A}^{+}_{N_-} = -\sin^2\left(\frac{\theta_\mathrm{I}}{2}\right) + \frac{4B_1}{ks}, \tag{C 20}$$

and then $\mathcal{A}^{+}_{N_+}$ and $\mathcal{A}^{-}_{N_-}$ are determined by finding the difference between the upper and lower signs of (C 6)

$$\mathcal{A}^{+}_{N_\pm} - \mathcal{A}^{-}_{N_\pm} = \pm\frac{4}{\mathrm{i}ks}\sum_{n=-\infty}^{\infty} n(\pm i)^n B_n, \tag{C 21}$$

which is simplified to $\mathcal{A}^{+}_{N_\pm} - \mathcal{A}^{-}_{N_\pm} = (8B_1/ks)$ when the truncation is applied. Finally, taking the difference between (C 18) and (C 19) yields

$$B_1(Z_1^{-1} + \hat{\sigma}_0 + \hat{\sigma}_2 - 8\mathrm{i}/(ks)) = \sin(\theta_\mathrm{I}). \tag{C 22}$$

Note that the presence of Z_1^{-1} in (C 22) means that B_1 is $O((ka)^2)$ (the scatterer size a does not appear in any other terms). Therefore, the factors $\pm 4B_1/(ks)$ represent small corrections (since $a < s/2$) and hence, the correct solution at low frequency is given by (2.10).

References

1. Movchan AB, Movchan NV, Jones IS, Colquitt DJ. 2017 *Mathematical modelling of waves in multi-scale structured media*. New York, NY: Chapman & Hall/CRC.
2. Craster RV, Guenneau S. 2013 *Acoustic metamaterials*. Berlin, Germany: Springer.
3. Cummer SA, Christensen J, Alù A. 2016 Controlling sound with acoustic metamaterials. *Nat. Rev. Mater.* **1**, 1–13. (doi:10.1038/natrevmats.2016.1)
4. Assouar B, Liang B, Wu Y, Li Y, Cheng JC, Jing Y. 2018 Acoustic metasurfaces. *Nat. Rev. Mater.* **3**, 460–472. (doi:10.1038/s41578-018-0061-4)
5. Liang B, Cheng JC, Qiu CW. 2018 Wavefront manipulation by acoustic metasurfaces: from physics and applications. *Nanophotonics* **7**, 1191–1205. (doi:10.1515/nanoph-2017-0122)
6. Mishuris GS, Movchan AB, Slepyan LI. 2019 Waves in elastic bodies with discrete and continuous dynamic microstructure. *Phil. Trans. R. Soc. A* **378**, 20190313. (doi:10.1098/rsta.2019.0313)
7. Schnitzer O, Brandão R. 2022 Absorption characteristics of large acoustic metasurfaces. *Phil. Trans. R. Soc. A* **380**, 20210399. (doi:10.1098/rsta.2021.0399)
8. Putley HJ, Guenneau S, Porter R, Craster RV. 2022 A tuneable electromagnetic metagrating. *Proc. R. Soc. A* **478**, 20220454. (doi:10.1098/rspa.2022.0454)
9. Millar RF. 1963 Plane wave spectra in grating theory: II. Scattering by an infinite grating of identical cylinders. *Can. J. Phys.* **41**, 2135–2154. (doi:10.1139/p63-209)
10. Scarpetta E, Sumbatyan MA. 1996 Explicit analytical results for one-mode oblique penetration into a periodic array of screens. *IMA J. Appl. Math.* **56**, 109–120. (doi:10.1093/imamat/56.2.109)
11. Bruno OP, Fernandez-Lado AG. 2017 Rapidly convergent quasi-periodic Green functions for scattering by arrays of cylinders—including Wood anomalies. *Proc. R. Soc. A* **473**, 20160802. (doi:10.1098/rspa.2016.0802)
12. Mishuris GS, Movchan AB, Slepyan LI. 2020 Localized waves at a line of dynamic inhomogeneities: general considerations and some specific problems. *J. Mech. Phys. Solids* **138**, 103901. (doi:10.1016/j.jmps.2020.103901)
13. Millar RF. 1964 Plane wave spectra in grating theory: III. Scattering by a semi-infinite grating of identical cylinders. *Can. J. Phys.* **42**, 1149–1184. (doi:10.1139/p64-107)
14. Hills NL, Karp SN. 1965 Semi-infinite diffraction gratings-I. *Commun. Pure Appl. Math.* **XVIII**, 203–233. (doi:10.1002/(ISSN)1097-0312)
15. Linton CM, Martin PA. 2004 Semi-infinite arrays of isotropic point scatterers. A unified approach. *SIAM J. Appl. Math.* **64**, 1035–1056. (doi:10.1137/S0036139903427891)
16. Lynott GM, Andrew V, Abrahams ID, Simon MJ, Parnell WJ, Assier RC. 2019 Acoustic scattering from a one-dimensional array; tail-end asymptotics for efficient evaluation of the quasi-periodic Green's function. *Wave Motion* **89**, 232–244. (doi:10.1016/j.wavemoti.2019.01.012)
17. Nethercote MA, Kisil AV, Assier RC. 2022 Diffraction of acoustic waves by a wedge of point scatterers. *SIAM J. Appl. Math.* **82**, 872–898. (doi:10.1137/21M1438608)
18. Wood RW. 1902 On a remarkable case of uneven distribution of light in a diffraction grating spectrum. *Proc. Phys. Soc.* **18**, 269–275. (doi:10.1088/1478-7814/18/1/325)
19. Rayleigh L. 1907 On the dynamical theory of gratings. *Proc. R. Soc. Lond. A* **79**, 399–416. (doi:10.1098/rspa.1907.0051)
20. Liu J, Declercq NF. 2015 Investigation of the origin of acoustic Wood anomaly. *J. Acoust. Soc. Am.* **138**, 1168–1179. (doi:10.1121/1.4926903)
21. Karp SN, Radlow J. 1956 On resonance in infinite gratings of cylinders. *IRE Trans. Antennas Propag.* **4**, 654–661. (doi:10.1109/TAP.1956.1144440)
22. Twersky V. 1952 On a multiple scattering theory of the finite grating and the wood anomalies. *J. Appl. Phys.* **23**, 1099–1118. (doi:10.1063/1.1701993)
23. Twersky V. 1956 On the scattering of waves by an infinite grating. *IRE Trans. Antennas Propag.* **4**, 330–345. (doi:10.1109/TAP.1956.1144408)
24. Twersky V. 1961 Multiple scattering of waves and optical phenomena. *J. Opt. Soc. Am.* **52**, 145–171. (doi:10.1364/JOSA.52.000145)
25. Twersky V. 1962 On the scattering of waves by an infinite grating of circular cylinders. *IRE Trans. Antennas Propag.* **10**, 737–765. (doi:10.1109/TAP.1962.1137940)
26. Millar RF. 1961a Scattering by a grating. I. *Can. J. Phys.* **39**, 81–103. (doi:10.1139/p61-007)

27. Millar RF. 1961b Scattering by a grating. II. *Can. J. Phys.* **39**, 104–118. (doi:10.1139/p61-008)
28. Linton CM, Thompson I. 2007 Resonant effects in scattering by periodic arrays. *Wave Motion* **44**, 165–175. (doi:10.1016/j.wavemoti.2006.09.002)
29. Millar RF. 1966 Plane wave spectra in grating theory: V. Scattering by a semi-infinite grating of isotropic scatterers. *Can. J. Phys.* **44**, 2839–2874. (doi:10.1139/p66-231)
30. Hills NL. 1965 Semi-infinite diffraction gratings-II. Inward resonance. *Commun. Pure Appl. Math.* **18**, 389–395. (doi:10.1002/(ISSN)1097-0312)
31. Millar RF. 1964 Plane wave spectra in grating theory: IV. Scattering by a finite grating of identical cylinders. *Can. J. Phys.* **42**, 2395–2410. (doi:10.1139/p64-218)
32. Bennetts LG, Peter MA, Montiel F. 2017 Localisation of Rayleigh-Bloch waves and damping of resonant loads on arrays of vertical cylinders. *J. Fluid Mech.* **813**, 508–527. (doi:10.1017/jfm.2016.855)
33. Evans DV, Porter R. 1999 Trapping and near-trapping by arrays of cylinders in waves. *J. Eng. Math.* **35**, 149–179. (doi:10.1023/A:1004358725444)
34. Odeh F. 1963 Uniqueness theorems for the Helmholtz equation in domains with infinite boundaries. *J. Math. Mech.* **12**, 857–867. (doi:10.1512/iumj.1963.12.12059)
35. Morgan RC, Karp SN. 1963 Uniqueness theorem for a surface wave problem in electromagnetic diffraction theory. *Commun. Pure Appl. Math.* **16**, 45–56. (doi:10.1002/(ISSN)1097-0312)
36. Evans DV, Porter R. 2002 On the existence of embedded surface waves along arrays of parallel plates. *Q. J. Mech. Appl. Math.* **55**, 481–494. (doi:10.1093/qjmam/55.3.481)
37. Linton CM, McIver M. 2002 The existence of Rayleigh-Bloch surface waves. *J. Fluid Mech.* **470**, 85–90. (doi:10.1017/S0022112002002227)
38. Linton CM, Porter R, Thompson I. 2007 Scattering by a semi-infinite periodic array and the excitation of surface waves. *SIAM J. Appl. Math.* **67**, 1233–1258. (doi:10.1137/060672662)
39. Antonakakis T, Craster RV, Guenneau S, Skelton EA. 2013 An asymptotic theory for waves guided by diffraction gratings or along microstructured surfaces. *Proc. R. Soc. A* **470**, 20130467. (doi:10.1098/rspa.2013.0467)
40. Bonnet-Ben Dhia A, Starling F. 1994 Guided waves by electromagnetic gratings and non-uniqueness examples for the diffraction problem. *Math. Methods Appl. Sci.* **17**, 305–338. (doi:10.1002/(ISSN)1099-1476)
41. Korolkov AI, Nazarov SA, Shanin AV. 2016 Stabilizing solutions at thresholds of the continuous spectrum and anomalous transmission of waves. *ZAMM Z. Angew. Math. Mech.* **96**, 1245–1260. (doi:10.1002/zamm.v96.10)
42. Shanin AV, Korolkov AI. 2017 Diffraction of a mode close to its cut-off by a transversal screen in a planar waveguide. *Wave Motion* **68**, 218–241. (doi:10.1016/j.wavemoti.2016.10.002)
43. Zalipaev VV, Popov MM. 1995 Wood's anomalies in the scattering problem of a plane wave on a smooth periodic boundary. *J. Math. Sci.* **73**, 353–360. (doi:10.1007/BF02362819)
44. Hewett DP, Hewitt IJ. 2016 Homogenized boundary conditions and resonance effects in Faraday cages. *Proc. R. Soc. A* **472**, 20160062. (doi:10.1098/rspa.2016.0062)
45. Touboul M, Lombard B, Bellis C. 2020a Time-domain simulation of wave propagation across resonant meta-interfaces. *J. Comput. Phys.* **414**, 1–39. (doi:10.1016/j.jcp.2020.109474)
46. Touboul M, Pham K, Maurel A, Marigo JJ, Lombard B, Bellis C. 2020 Effective resonant model and simulations in the time-domain of wave scattering from a periodic row of highly-contrasted inclusions. *J. Elast.* **142**, 53–82. (doi:10.1007/s10659-020-09789-2)
47. Foldy LL. 1945 The multiple scattering of waves. I. General theory of isotropic scattering by randomly distributed scatterers. *Phys. Rev.* **67**, 107–119. (doi:10.1103/PhysRev.67.107)
48. Olver FWJ*et al.* NIST digital library of mathematical functions.
49. Gradshteyn IS, Ryzhik IM. 2014 *Table of integrals, series, and products*, 8th edn. New York, NY: Academic Press.
50. Nethercote MA, Assier RC, Abrahams ID. 2020 Analytical methods for perfect wedge diffraction: a review. *Wave Motion* **93**, 102479. (doi:10.1016/j.wavemoti.2019.102479)
51. Noble B. 1958 *Methods based on the Wiener-Hopf Technique for the solution of partial differential equations (1988 reprint)*. New York, NY: Chelsea Publishing Company.
52. Gorbushin N, Nguyen VH, Parnell WJ, Assier RC, Naili S. 2019 Transient thermal boundary value problems in the half-space with mixed convective boundary conditions. *J. Eng. Math.* **114**, 141–158. (doi:10.1007/s10665-019-09986-6)

53. Martin PA. 2006 *Multiple scattering: interaction of time-harmonic waves with N obstacles*. Cambridge, UK: Cambridge University Press.
54. Linton CM. 2010 Lattice sums for the Helmhoitz equation. *SIAM Rev.* **52**, 630–674. (doi:10.1137/09075130X)
55. Jones DS. 1964 *The theory of electromagnetism*. London, UK: Pergamon Press.
56. Thompson I, Linton CM. 2007 On the excitation of a closely spaced array by a line source. *IMA J. Appl. Math.* **72**, 476–497. (doi:10.1093/imamat/hxm014)